



Development of novel AMP-based absorbents for efficient CO₂ capture with low energy consumption through modifying the electrostatic potential

Guanchu Lu ^{a,1}, Zhe Wang ^{a,1}, Zongyang Yue ^a, Wenjing Wei ^a, Yi Huang ^a, Xiaolei Zhang ^b, Xianfeng Fan ^{a,*}

^a Institute for Materials and Processes, School of Engineering, the University of Edinburgh, Edinburgh EH9 3FB, Scotland, UK

^b Chemical and Process Engineering, University of Strathclyde, Glasgow G1 1XQ, Scotland, UK



ARTICLE INFO

Keywords:

Non-aqueous absorbents
CO₂ capture
Low energy regeneration
Polar solvents
Amines

ABSTRACT

The global deployment of aqueous amine absorbents for carbon dioxide (CO₂) capture is hindered by their high energy consumption. A potential solution to this challenge lies in the utilization of non-aqueous amine systems, which offer energy-efficient alternatives. However, they are prone to form precipitation during CO₂ absorption process, which limits their application. Combining experimental and theoretical studies, we found that the electrostatic potential of carbamate, instead of van der Waals force, is a major factor controlling the precipitation, and hydrogen bonds can effectively reduce the electrostatic potential of carbamate and prevent precipitation. Single solvent screening experiments have also demonstrated that the absorption rate is closely related to the viscosity of the organic solvent and the affinity of the functional group for CO₂. The polar solvents (Dimethylformamide (DMF), Dimethyl sulfoxide (DMSO), and N-Methylformamide (NMF)) exhibit higher absorption rates, but suffer from issues of precipitation. Hydroxyl group riched solvents (Ethylene glycol (EG) and Glycerol) exhibit lower absorption rate, but they don't have the issue of precipitation. Based on these findings, several novel 2-Amino-2-methyl-1-propanol (AMP)-based non-aqueous absorbents have been developed aiming at reducing the energy penalty, and improving CO₂ absorption and desorption performance. Among these absorbents, AMP-EG-DMF (4–3) exhibits maximum CO₂ absorption rate and absorption capacity of 9.91 g-CO₂/(kg-soln.-min.) and 122 g-CO₂/(kg-soln.), respectively, which are 64.1% and 28.4% higher than those of 30 wt% AMP aqueous solution, respectively. Additionally, compared to 30 wt% MEA, the energy consumption of AMP-EG-DMF (4–3) shows 46.30% reduction. The addition of EG effectively improves the electrostatic solubility of AMP-carbamate by increasing the number and strength of hydrogen bonds, thus avoiding the generation of precipitation. The final product species and reaction mechanism were analysed by using ¹³C and ¹H NMR, In-situ ATR-FTIR, and quantum chemical calculation. The combination of theoretical and experimental results indicates that bi-solvent AMP-based absorbents can serve as a promising alternative for low-energy CO₂ capture.

1. Introduction

Climate change caused by greenhouse gas emissions is one of the major issues in modern society. As a typical greenhouse gas, CO₂ concentration in the atmosphere has grown by 46% from 280 ppm in the preindustrial era to over 410 ppm in 2020, which is responsible for 80% of all greenhouse gas release. Carbon capture, utilisation and storage

(CCUS) have been regarded as a promising technique to reduce greenhouse gas emissions [1,2], and CO₂ capture is the core technology of CCUS and accounts for over 70% of the total operating costs [3]. Considering its low price and fast reaction rate with CO₂, 30 wt% aqueous MEA has been adopted as the benchmark for CO₂ capture in commercialisation [4]. However, the shortcomings of this method are the high corrosion and degradation rate, and high energy consumption for solvent regeneration, which is mainly due to the use of water as

Abbreviations: AMP, 2-Amino-2-methyl-1-propanol; MEA, Monoethanolamine; DMF, Dimethylformamide; NMF, N-Methylformamide; DMSO, Dimethyl sulfoxide; EG, Ethylene glycol; NMR, Nuclear magnetic resonance; ATR, Attenuated total reflection; ESP, Electrostatic potential; DEGMEE, 2-(2-Ethoxyethoxy)ethanol; DFT, Density functional theory; DSC, Differential Scanning Calorimetry; TGA, Thermogravimetric Analyzer; FT-IR, Fourier-transform infrared spectroscopy.

* Corresponding author.

E-mail address: x.fan@ed.ac.uk (X. Fan).

¹ These authors contributed equally.

<https://doi.org/10.1016/j.cej.2023.145929>

Received 26 June 2023; Received in revised form 31 August 2023; Accepted 6 September 2023

Available online 9 September 2023

1385-8947/© 2023 The Authors. Published by Elsevier B.V. This is an open access article under the CC BY license (<http://creativecommons.org/licenses/by/4.0/>).

Nomenclature	
r_{abs}	Absorption rate of CO ₂ (g-CO ₂ /(kg-soln. ·min.)),
r_{des}	Desorption rate of CO ₂ (g-CO ₂ /(kg-soln. ·min.)),
a_{abs}	Absorption amount of CO ₂ (g-CO ₂ /kg-soln.).
α_{des}	Desorption amount of CO ₂ (g-CO ₂ /kg-soln.).
Q	Regeneration energy (kJ)
Q_s	Sensible heat (kJ)
Q_r	Reaction heat of desorption (kJ)
Q_v	Latent heat of vaporization (kJ)
EC	Ratio of energy/released CO ₂ (kJ/mol),
C_p	Specific heat capacity (kJ/kg ⁻¹ • K ⁻¹),
ΔT	Temperature difference between the top and bottom of the stripper (K)
ΔH	Reaction heat (kJ/mol)
n_w	Molar ratio of water
n_{CO_2}	Molar ratio of CO ₂
C_A	Absorbent concentration (mole/L)
k	Reaction rate coefficient (min ⁻¹)
k_0	Pre-exponential factor (min ⁻¹)
E_a	Activation energy (J/mol)
R	Ideal gas constant (8.314 J/mole/K)
T	Temperature (°C)
η	Desorption efficiency (%)

solvent [5].

Developing new absorbents by replacing water with organic solvents has attracted significant academic and industrial attention. Organic solvents, including alcohols [6–8], glycols [9–13], glycol ethers [14–17], glymes [18], pyrrolidones [19,20], formamides [21,22], and sulfoxides [23–25] have proven to be a promising solution for reducing regeneration energy. These are due to their lower specific heat capacity, lower heat of vaporization, and higher boiling points compared to water [26]. However, using a single organic solvent can result in unexpected problems. High-volatility alcohols, such as methanol and ethanol, can lead to significant solvent loss when processing large-scale flue gases, resulting in both economic loss and environmental pollution. Glycols like EG, DEG, and TEG have non-linear increases in viscosity during the CO₂ absorption process, leading to lower absorption rates. Polar organics such as formamides, pyrrolidones and sulfoxides could effectively enhance CO₂ absorption rate, but they are prone to form precipitate during the absorption process, which causes clogging in the pipelines and absorption efficiency reduced.

In short, single organic solvent is hard to meet the all the requirements of non-aqueous amine absorbents. The combination of different solvents could be able to solve this problem effectively. Therefore, a bi-solvent system with a buffered solvent has been introduced to solve these problems, but few studies has been reported in literature. Barbarossa et al. [27] studied the non-aqueous systems formed by 2-amino-2-methyl-1-propanol (AMP) dissolved in alcohol mixtures (ethylene glycol (EG) and ethanol or 1-propanol) with a volume ratio of 1:1. The addition of ethanol or 1-propanol as buffer solvents could effectively reduce the viscosity of the absorbents. Their results showed that these two absorbents had high loading capacities around 0.9 mol (CO₂)/mole (Amine) and could be regenerated under 80–90 °C. Wagaarachchige et al. [28] proposed a low-viscosity non-aqueous binary solvents blend for reversible CO₂ capture. In their study, non-aqueous diisopropylamine (DPA) solutions were prepared by mixing 30 wt% DPA, 35 wt% methanol, and 35 wt% sulfolane. Methanol was selected as a buffer solvent due to its low boiling point, low viscosity, and low corrosivity, providing a high CO₂-rich loading up to 0.88 mol CO₂/mole amine and a high CO₂ cyclic capacity of 0.48 mol (CO₂)/mole amine. Overall, in previous research, the buffer solvents were limited to volatile low-carbon alcohols which resulted in additional cost due to solvent evaporation, and the effect of the mass or volume ratio of the two solvents on the absorption performance has not been optimized.

The CO₂ absorbent developed in this work consists of AMP and two other non-aqueous solvents. AMP is chosen as the basic component due to its lower reaction heat required for CO₂ regeneration, excellent thermal and oxidative stability, and lower corrosion rates on steel equipment compared to MEA, despite its relatively slow absorption kinetics in both aqueous and non-aqueous solutions. CO₂ is known to react with AMP to form insoluble precipitates in most non-aqueous solvents. This limits its application in CO₂ capture [25,29]. If precipitation problem of AMP absorbents can be solved, they might become an

excellent recipe of CO₂ adsorbents with high capture efficiency and low energy consumption. Furthermore, the capital cost of absorption column for the use of AMP absorbents can be reduced due to avoid of the precipitate separation. In this study, we firstly combined experimental and theoretical studies to understand the precipitation mechanism of AMP carbamate through molecular dynamics simulations and DFT calculations. The results indicate that electrostatic interaction between AMP carbamate and solvents is a major factor controlling the precipitation. Based on this theory, organic solvents which can form hydrogen bonds with AMP carbamate will be investigated to reduce the electrostatic interaction to mitigate the precipitation. In the meanwhile, solvents must have high boiling points and low vapor pressures, such as alcohols, glycols, glycol ethers, glycerol, formamides, and sulfoxides. CO₂ absorption performance of these single-solvent AMP absorbents is firstly tested, and the promising solvents are selected for the formation of bi-solvent absorbents. The mass ratios of the binary solvents are optimized to enhance their synergism with AMP to improve the absorption capacity and reduce the energy consumption. The CO₂ absorption rate and capacity, desorption rate and efficiency, cyclic stability, and energy consumption of the absorbents are thoroughly investigated and compared with MEA-H₂O. Finally, various analytical techniques, such as ¹³C nuclear magnetic resonance (¹³C NMR) analysis, Fourier-transform infrared spectroscopy (FT-IR) analysis, and quantum chemical calculation (Gaussian09), are utilised to elucidate the CO₂ absorption mechanism into the non-aqueous bi-solvent and AMP absorbents. The results indicate that the non-aqueous bi-solvent AMP absorbent can maintain as liquid phase during the CO₂ absorption and exhibit a high absorption rate, high absorption capacity, and sufficient regeneration efficiency below 90 °C. Overall, this study provides a novel bi-solvent strategy to address the precipitation issue in CO₂ absorption processes, particularly for non-aqueous amine absorbents, such as AMP-based absorbents. The detailed investigation and analysis of the CO₂ absorption mechanism provide a comprehensive understanding of the bi-solvent approach's efficacy and may aid in developing more efficient and effective CO₂ capture technologies.

2. Materials and experimental sections

2.1. Materials

2-Amino-2-methyl-1-propanol (AMP, 99%), Monoethanolamine (MEA, 99%), Diethylene glycol monoethyl ether (DEGMEE, 98+%), N-Methylformamide (NMF, 99%), and N, N-Dimethylformamide (DMF, 99%) were provided by ACROS organics. 1-Butanol (1-BuOH, ≥99.4%), Ethylene glycol (EG, ≥99.0%), and Dimethyl sulfoxide (DMSO, ≥99.0%) were provided by Sigma-Aldrich. Glycerol (99+%) was provided by Alfa Aesar. All the reagents were used without further purification. Absorbents were prepared by gravimetric method, using a Sartorius ED224S balance with an accuracy of ± 1 × 10⁻⁴ g and an uncertainty of less than 0.1 wt%. 1.5 g of AMP was dissolved in 3.5 g single or bi-solvent system.

Gases used for absorption and desorption experiments (CO_2 and N_2) were purchased from Linde Group UK with a minimum purity of 99.99%. A mixture of 20% CO_2 and 80% N_2 was used to mimic the flue gas.

2.2. Absorption and desorption setup

The batch experiments of CO_2 absorption (25°C)-desorption ($50\text{--}90^\circ\text{C}$) were performed at near atmospheric pressure in a lab-scale apparatus as described in our previous work, hence only a brief introduction will be given here [30,31]. Fig. S1 illustrates the CO_2 capture setup, comprising a cylindrical quartz reactor (14 mm inner diameter, 1.5 mm wall thickness) and the measurement of CO_2 concentration and flowrate. The absorbent was prepared and placed inside the quartz reactor. Simulated flue gas was introduced at the bottom of the solution through a small quartz tube, with a total flow rate of 200 ml/min regulated by two calibrated mass flow controllers (Brooks Instruments GF-Series, N_2 range: 0–400 ml/min, CO_2 range: 0–100 ml/min). A non-dispersive infrared CO_2 sensor (COZIR-W-100, CO_2 calibration range: 0–70% v/v), and finally a mass flow meter (Brooks Instruments SLA5860, range: 0–500 ml/min). The self-programmed Labview data collection software was utilised to record the monitored variables (temperature, flow rate, humidity and CO_2 concentration) every second from the beginning of the absorption experiment. All gas lines were swept with N_2 before and between experiments. The absorption experiments were conducted under standard atmospheric pressure and room temperature conditions.

The CO_2 -loaded AMP-based absorbents were regenerated after the absorption step using microwave irradiation in the same quartz reactor as the absorption experiments. The setup for desorption is depicted in Fig. S2. A magnetron operating at 2.45 GHz, controlled by an Alter SM445 power supply with a maximum output power of 1.2 kW, generated the microwave. The forward and reflected microwave power flow were measured using a dual-directional coupler (GAE Inc., GA310x). The temperature of the solution was continuously monitored at the centre of the liquid bulk using a fibre optic sensor probe (Opsens OTG-MPK8). The microwave source was initially set to 0.1 kW power to raise the solution's temperature from ambient to the desired regeneration temperature. The power was then manually adjusted to maintain a constant temperature throughout the process.

2.3. Experimental procedures

The experimental work is divided into three distinct parts. The first part was designed to develop a recipe of organic solvents and AMP mixture to avoid the precipitation of CO_2 reaction product through reducing the electrostatic potential. In the second part, DMF, DMSO, and NMF were selected to mix with EG to form bi-solvent system to improve CO_2 absorption performance and reduce the regeneration energy. The solutions were regenerated at a temperature ranging from 50 to 90 °C. The cyclic stability of the best solutions was then investigated to simulate the industrial CO_2 capture process. In the third part, the reaction mechanism, thermal stability, energy consumption calculation, and characterization were studied. The physical properties of these chemicals are summarized and presented in Table S1.

2.4. Calculation and analysis methods

2.4.1. Molecular dynamics simulation

For simulating a real reaction condition and understanding the precipitation mechanism of AMP– CO_2 products in non-aqueous solvents, amorphous cells were constructed with AMP products with different solvents in Material Studio 2020. The van der Waals solubility, electrostatic solubility and hydrogen bonding strength were elucidated [22]. The calculation details are concluded at supporting information part 3.

2.4.2. Absorption and desorption calculation

The absorption and desorption rate and capacity were calculated by Eqs. (1)–(4). Where r_{abs} and r_{des} is reaction rate of absorption and desorption (g- CO_2 /(kg-soln. ·min.)), a_{abs} and α_{des} is the CO_2 absorption and desorption capacity (g- CO_2 /kg-soln.).

$$r_{abs} = \frac{(y_{\text{CO}_2}^{\text{in}} - y_{\text{CO}_2}^{\text{out}})M_{\text{CO}_2}}{M_{\text{air}}} * \frac{273}{273 + T_{abs}} * \frac{P_{abs}}{101.25} \quad (1)$$

$$r_{des} = \frac{(y_{\text{CO}_2}^{\text{out}})M_{\text{CO}_2}}{M_{\text{air}}} * \frac{273}{273 + T_{abs}} * \frac{P_{des}}{101.25} \quad (2)$$

$$\alpha_{abs} = \int_0^t r_{abs} dt \quad (3)$$

$$\alpha_{des} = \int_0^t r_{des} dt \quad (4)$$

2.4.3. Estimation of CO_2 desorption energy

The CO_2 desorption is the major energy-consuming process in CO_2 capture [32,33]. The regeneration energy (Q) consists of three parts: the reaction heat of desorption (Q_r), the latent heat of vaporization (Q_v), and the sensible heat (Q_s). EC is defined as the ratio of energy/released CO_2 . The calculation formulas are shown below:

$$Q = Q_s + Q_r + Q_v \quad (5)$$

$$EC = \frac{\text{Energy(KJ)}}{\text{CO}_2\text{stripped(mol)}} \quad (6)$$

2.4.4. Characterization analysis

2.4.4.1. NMR. The ^{13}C and ^1H spectrum of AMP-based absorbents are analysed by a 500 MHZ nuclear magnetic resonance spectrometer (Buker Ascend NMR AVA500). To provide enough signals for the deuterium lock, deuterated D_2O was introduced into the NMR tube [33]. When preparing the samples, 0.2 ml AMP-based absorbents and 0.2 ml D_2O were mixed in plastic centrifuge tube and inject into Kimble NMR sample tubes (500 MHZ). The NMR tubes then send to the automation NMR spectrometer for ^{13}C spectrum (64 scan) and ^1H spectrum (8 scan).

2.4.4.2. ATR FT-IR. The composition of AMP-based absorbents in the reaction process was analysed by a PerkinElmer Frontier spectrometer equipped with a universal ATR (Attenuated Total Reflection) polarization accessory. In each IR characterization, 0.25 ml samples were placed onto the ATR crystal, then scanned with 50 accumulations. The measurement is taken, and, after completion, the crystal is wiped clean using ethanol and water. The wavenumbers ranged from 650 cm^{-1} to 4000 cm^{-1} .

2.4.4.3. TG/DSC. In this study, thermogravimetric (TG) analysis was employed to measure the weight change and thermal stability during desorption process with synchronous thermal analyzer (NETZSCH STA 449 F1). The fresh and CO_2 -saturated absorbents were measured were observed in 5 ml/min N_2 atmosphere under 90°C for 60 min, and temperature rise rate is 5 K per minute. In each TG analysis, 20 mg samples were placed into aluminium pan with lid, with one hole on the top. The weight change during heating is observed. As the gas stream containing CO_2 bubbled through the absorbents from 25°C with a flow rate of 20 ml/min, temperature rise rate is 1 K per minute and final temperature is 40°C . The synchronous thermal analyzer was employed to measure the weight change and heat effect of absorbents during absorption. Similar as TG analysis, 20 mg samples were placed into open aluminium pan, for fully contact with CO_2 during measurement. Therefore, the reaction heat and volatility could be estimated [32,33].

2.4.5. Quantum computational methods

Molecular simulation provides a detailed understanding of the molecular-level interactions between gases and absorbents. In this study, all calculations were performed using the Gaussian 09 software package [34], utilizing density functional theory (DFT) as a powerful tool to elucidate the precipitation and reaction mechanism. The geometries, frequencies and single point energy of reactants and products were optimized at the B3LYP/6-311+G (d, p) level. Also, natural valence bond orbital theory (NBO) charge analysis of AMP-CO₂ products are performed in same level calculation [35].

Results and discussion

3.1. Mitigation of the precipitation for AMP-CO₂ absorption products

Non-aqueous AMP absorbent has attracted much attention as its low vapour pressure and low CO₂ desorption energy required. However, the reaction product of CO₂ with AMP forms precipitates in most of organic solvents, limit their CO₂ capture capacity, and cannot be recycled in a cyclic CO₂ capture process. Typically, CO₂ absorption by non-aqueous AMP stops when the CO₂ loading reaches only 10–30% of the capacity, depending on the solvent used. The strategy here is to find a proper solvent to modify intermolecular force to prevent the precipitation of CO₂-AMP products, and maximize the adsorption potential of AMP based absorbents for efficient CO₂ capture. A series of batch experiments and theoretical calculations were designed to test the impact of various solvents on the CO₂ absorption performance of AMP and on the precipitation of AMP-CO₂ products. The CO₂ absorption behaviour of 30 wt % AMP aqueous solution was measured as a reference. In general, most of the AMP-based absorbents underwent precipitation when their CO₂ absorption capacity higher than 30 g-CO₂/(kg-soln.). Only H₂O, EG, and glycerol are excluded.

With the absorption progress, the AMP-CO₂ products gradually displayed a turbid appearance, the precipitates are then formed and ultimately obstructed the gas inlet tube and impeded CO₂ absorption. During the CO₂ absorption process, measurements were recorded until absorption ceased for precipitated systems, whereas for non-precipitated systems, measurements were taken for up to 50 min. This period is sufficient for most of the absorbents to reach equilibrium. However, in some cases, this absorption time was not adequate to reach the maximum absorption limit. For a fair comparison, the desorption time of 50 min was used as most absorbents have reached the equilibrium at this

time [36,37].

As shown in the Fig. 1, AMP mixtures with water, EG or glycerol do not form precipitation but have a low CO₂ absorption rate. While AMP mixtures with DMF, DMSO, NMF, DEGMEE or 1-Butanol have a much faster CO₂ absorption rate, but formed precipitates. The precipitation terminates CO₂ absorption at its early stage and results in a low absorption capacity. The maximum absorption rates of AMP mixture with DMF, DMSO and NMF are about 16.0, 15.9 and 14.5 g-CO₂/ (kg-soln.·min.) respectively. Due to the carbamate precipitation during CO₂ absorption, their total CO₂ uptakes of AMP mixed with DMF, DMSO and NMF are only 72, 88 and 73 g-CO₂/(kg-soln.), respectively. On the contrary, in the non-precipitated group, AMP mixed with H₂O and EG have high CO₂ absorption capacity even though their maximum absorption rates were only 5.9 and 5.2 g-CO₂/(kg-soln.·min.), much lower than that of AMP mixed with DMF, DMSO and NMF. This means that AMP mixed with DMF, DMSO and NMF has potential to achieve a much higher CO₂ absorption capacity if the precipitation can be prevented. The functional groups of the solvents should have a decisive influence on the precipitation and CO₂ absorption capacity. Both the sulfoxide group and the sulphur group could produce precipitation during CO₂ absorption, but the multi-hydroxyl group not. According to the previous research, the components of AMP-CO₂ products crystal is research thoroughly [38], which contains AMPH⁺ and AMPCO₃²⁻.

The CO₂ absorption rate and the CO₂ adsorption capacity are also determined by the solvent's viscosity and functional groups. A high viscosity leads to a decrease in absorption rate due to slow gas-liquid mass transfer between the liquid and vapour phases. For instance, glycerol has the lowest maximum absorption rate due to its high viscosity (1.412 Pa·s) [39]. However, there are some exceptions, for example DEGMEE has a higher viscosity but also a higher absorption rate than 1-butanol. The exceptions indicate that the functional group also plays a critical role in the CO₂ absorption process. Certain functional groups, such as carbonyl, sulfoxide, and ether groups, have high CO₂-affinity, whereas hydroxyl groups are not conducive to CO₂ absorption, which is consistent with the previous research [15]. Therefore, the higher CO₂ absorption rate and capacity of DEGMEE can be attributed to the strong CO₂-affinity to the ether groups in its molecule, compared to 1-butanol. Additionally, when comparing DMF and NMF, it was found that the CO₂ uptake of AMP-NMF is slightly higher than that of AMP-DMF. However, the maximum absorption rate of AMP-NMF is much lower than that of AMP-DMF. This can be explained by the fact that the -NH group in the NMF molecule leads to a competitive reaction

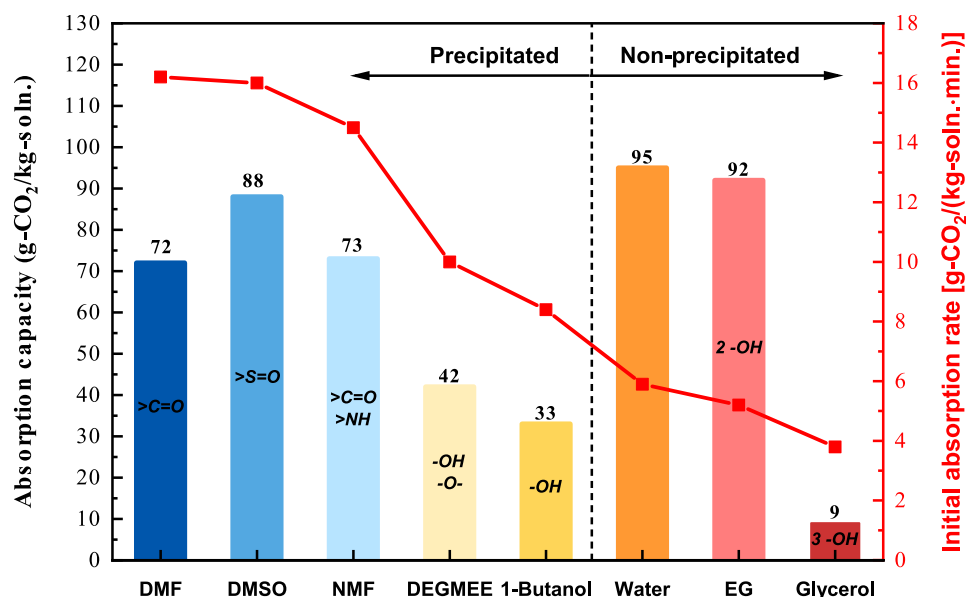


Fig. 1. Effect of solvents with different functional groups on CO₂ absorption of AMP mixtures. (30% AMP, Absorption temperature: 25°C).

with CO_2 to increase absorption, but it also forms hydrogen bonds, leading to an increase in viscosity and a decrease in absorption rate.

3.2. The mechanism of AMP carbamate precipitation

In order to maximize the potential of the absorbents which consist of DMF/DMSO/NMF with AMP through mitigating the negative effect

from carbamate precipitation. Considering the solvents with hydroxyl groups (EG, glycerol) could weaken the intermolecular forces to prevent AMP-carbamate precipitation during CO_2 absorption, we assumed that hydrogen bonds formed by solvents could enhance the solubility of AMP- CO_2 products. Therefore, a molecular dynamics simulation is performed for calculating the hydrogen bonds and solubility parameters of AMP with different solvents.

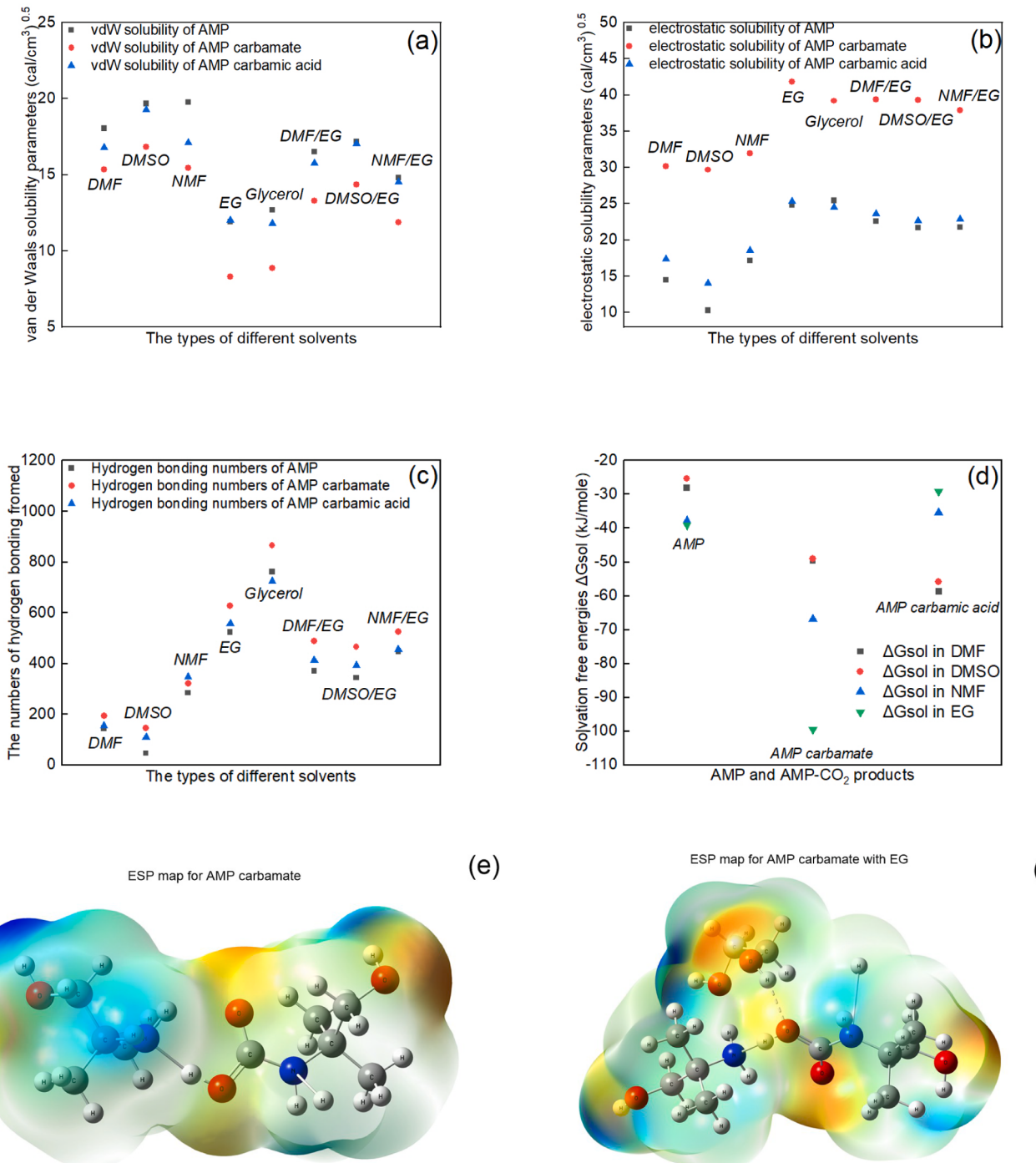


Fig. 2. The results of MD simulation and Quantum calculation. a) vdW solubility of AMP and AMP-CO₂ products in various solvents. b) electrostatic solubility of AMP and AMP-CO₂ products in various solvents. c) H-bonding numbers of AMP and AMP-CO₂ products in various solvents. d) solvation free energy of AMP and AMP-CO₂ products in various solvents. e) ESP map for AMP carbamate. f) ESP map for AMP carbamate-EG complex.

The composition of the precipitate during CO₂ capture process using AMP absorbents has already been confirmed by previous research [38]. As seen in Eq. (7) below, CO₂ dissolved into the solution and reacted with AMP forming AMP-carbamate (RNHC⁻) and protonated AMP (RNH₃⁺) [40]. With the CO₂ capture progressed, the precipitated solid crystal (RNH₃⁺ RNHC⁻) is formed through ionic interaction, and cannot be dispersed in some of the organic solvents. In molecular dynamics simulation, we separately calculated the van der Waals solubility parameters, electrostatic solubility parameters, and hydrogen bond strength of AMP, AMP carbamate, and AMP carbamic acid in different solvents. The results are presented in Fig. 2(a), (b), (c). The detailed data can be found in the supporting information part 3.



Van der Waals solubility parameters, electrostatic solubility parameters and hydrogen bonding numbers can be used to understand the dissolution of AMP carbamate in solvents. Theoretically, polar solvents such as DMF, DMSO and NMF have been regarded as ‘universal solvent’ due to their high polarity and ability to dissolve various compounds. DMF, DMSO and NMF should dissolve AMP carbamate complex better than glycerol and glycol based on their van der Waals solubility parameters (Fig. 2a). Surprisingly, our experimental results contradict this assumption, i.e. glycerol and glycol dissolve AMP carbamate complex better than DMF, DMSO and NMF. This means that van der Waals solubility parameters is not a major parameter controlling the solubility of AMP carbamate. After examining electrostatic solubility parameters and hydrogen bonding numbers (Fig. 2b and Fig. 2c), we find that the electrostatic solubility parameters of EG and glycerol are 40% to 42% higher than that of DMF, DMSO, and NMF. The hydrogen bonding numbers of EG and glycerol are 48% to 83% higher than these of DMF, DMSO, and NMF. This means that electrostatic solubility parameters and hydrogen bond might be the major factors controlling the solubility of AMP carbamate. The abundant hydrogen bonds formed between EG/glycerol and the AMP carbamate lead to a reduction in the electrostatic potential and intramolecular force of AMP carbamates (RNH₃⁺ RNHC⁻), therefore preventing their precipitation. To verify this assumption, we calculated the solvation free energy (ΔG_{sol}) of AMP carbamate in various solvents [41], as shown in Fig. 2(d). The results indicate that the solvation free energy of AMP carbamate in EG is significantly lower (-99 kJ/mole) than in other solvents. Furthermore, an electrostatic potential (ESP) map demonstrates that EG effectively weakens the potential energy of AMP carbamate, and the Maximum electrostatic potential of AMP carbamate decreases from -151.94 to -162.83 kJ/mole. Thus, it can be concluded that the electrostatic force plays a crucial role and the van der Waals force (London dispersion force) is not the critical factor for dissolving carbamates.

Based on above analysis, a novel strategy is proposed to prevent the precipitation of AMP carbamate in non-aqueous absorbents and improve the CO₂ adsorption capacity of AMP-based absorbents. This strategy involves enhancing hydrogen bonding and reducing the electrostatic potential of AMP carbamate. EG and glycerol are recommended additives due to their multi-hydroxyl groups, which strengthen hydrogen bond formation in the absorbent mixture and prevent precipitation. Considering absorption capacity and rate, EG is superior to glycerol as a second solvent. EG will be used as the second solvents to develop and optimize a novel bi-solvent AMP absorbent in this study. Our simulation results in Fig. 2(a), (b), (c) have demonstrated that the addition of EG increases solubility parameters and the number of hydrogen bonds of AMP based adsorbents. As the combination of AMP with DMF, DMSO, and NMF already exhibits a high CO₂ absorption rate, the addition of EG to the mixture is for reducing the intermolecular force of AMP carbamate, thereby preventing the formation of precipitates. Experimental work designed in following section is to realize this strategy.

3.2. Absorption performance of bi-solvent AMP absorbents

3.2.1. The absorption performance of AMP-based absorbents

As discussed in section 2.3, the potential benefits of combining EG with DMF, NMF, and DMSO to form bi-solvent AMP-based absorbents may give a high CO₂ absorption capacity and prevent precipitation. To investigate the impact of both solvent type and mass ratio on absorption performance, a series of experiments were conducted by varying the mass ratios of EG to DMF, DMSO, or NMF while maintaining a constant mass proportion of 30 wt% AMP. The specific mass ratios used in the study are presented in Table 1.

As depicted in Fig. 3 (a)-(f), the absorption curves of all AMP-based bi-solvent absorbents exhibited a similar trend, wherein the absorption rate declined rapidly from its peak value over time before stabilizing at the end. The absorbents consisting of AMP mixed with pure DMF, NMF, or DMSO demonstrated the highest CO₂ absorption rate before precipitation occurred, while AMP mixed with pure EG had the lowest absorption rate. The addition of EG into AMP-(DMF/NMF/DMSO) system forms a bi-solvent AMP absorbent. The maximum absorption rate of the bi-solvent AMP absorbents increased with a decrease in EG mass proportion, indicating that the addition of DMF, NMF, or DMSO solvents effectively resolved the issue of low absorption rates as observed in pure AMP-EG absorbent. However, when the EG concentration was less than 40 wt%, precipitation still occurred in all three bi-solvent systems during CO₂ absorption, as illustrated in Fig. 4.

As can be seen from Fig. 3, increase in EG proportion in the bi-solvent led to a delay of the precipitation for all three systems, suggesting that EG exhibited an inhibitory effect on precipitation. Once EG mass ratio reaching 40 wt%, none of these three bi-solvent systems produced precipitates during the CO₂ capture process. At the same time, the CO₂ absorption capacity of the three absorbents at this ratio were the largest in their respective systems. Additionally, based on the t₉₅ data in Table 2, it can be seen that bi-solvent AMP absorbents at a mass ratio of 4–3 exhibited the shortest time to reach 95% absorption uptake in their respective systems. Therefore, we could consider that the mass ratio of AMP: EG: (DMF/NMF/EG) equals to 3:4:3 is the optimal mass ratio for all three systems.

Fig. 4 shows the effect of mass fraction of polar solvents (DMF/DMSO/NMF) on the time when precipitation occurs. The results indicate that with the mass fraction of polar solvent increases, the time taken for the precipitation formation decreases. Among these absorbents, the shortest time for precipitation formation is occurred in AMP-DMF solvent system, which means that the AMP-carbamate produced by the reaction in DMF is very fast. This type of precipitation can be effectively inhibited by EG, once the proportion of EG is 40 wt%, the precipitation no longer occurs.

3.2.2. The absorption performance of AMP-based absorbents and MEA

30 wt% aqueous MEA has been seen as a benchmark absorbent for industrial CO₂ capture. To determine whether the bi-solvent AMP-based absorbents could perform comparably, single-solvent absorbents (aqueous MEA, aqueous AMP and AMP-EG) were firstly investigated. Fig. 5 shows that in the single-solvent systems, MEA-H₂O outperformed AMP-H₂O and AMP-EG absorbents in both maximum absorption rate and absorption capacity, and the maximum absorption rate and absorption capacity of AMP-EG were the lowest. This is likely due to the steric hindrance effect in the AMP molecule [20]. The performance of AMP-EG was improved considerably after the addition of DMF, DMSO, or NMF to form bi-solvent absorbents. Compared with the single-solvent AMP-EG absorbent, the bi-solvent system of AMP-EG-DMF (4–3), AMP-EG-NMF (4–3) and AMP-EG-DMSO (4–3) have more than doubled maximum absorption rates and CO₂ uptake increased by more than 20%. Among these three bi-solvent systems, AMP-EG-DMF (4–3) performed the best with maximum CO₂ absorption rate and absorption capacity of 9.91 g·CO₂/ (kg-soln. ·min.) and 122 g·CO₂/ (kg-soln.), respectively.

Table 1

Composition of the absorbents and their denotes in this study.

30 % AMP –based Absorbent	EG mass ratio	DMF or DMSO or NMF mass ratio	Denote
AMP-EG-DMF or AMP-EG-DMSO or AMP-EG-NMF	0%	70%	0-7
	10%	60%	1-6
	20%	50%	2-5
	30%	40%	3-4
	40%	30%	4-3
	50%	20%	5-4
	60%	10%	6-1
	70%	0%	7-0

3.3. Desorption performance of bi-solvent AMP-based absorbents

3.3.1. The desorption performance of AMP-based absorbents

CO_2 desorption performance is an important criterion of absorbents. Therefore, we further investigated the desorption properties of the three bi-solvent systems with the mass ratio of AMP: EG: polar solvents of 3:4:3 (4–3), and took 30 wt% AMP-EG as a comparison. As shown in Fig. 6, temperature plays an important role in the CO_2 desorption process. In general, the desorption rates of AMP-based absorbents show a log-normal trend along with the regeneration time. The desorption rate increases with increasing temperature. Among the AMP-based absorbents, AMP-EG-DMF exhibits the highest maximum desorption rate of 52.9 g- CO_2 / (kg-soln. ·min.) at 90 °C, which is more than twice that of AMP-EG at the same regeneration temperature. According to the summarized results in Table 3, the CO_2 desorption efficiency increases with the regeneration temperature increases. The order of regeneration efficiency of AMP based absorbents was AMP-EG-DMF (4–3) > AMP-EG-NMF (4–3) > AMP-EG-DMSO (4–3). AMP-EG-DMF (4–3) could reach 97.8% regeneration efficiency at 90 °C, which indicates that the bi-solvent AMP-based absorbents have the ability to fully regenerate at 90 °C. This results in a noteworthy 25% reduction in regeneration temperature compared to that of the 30 wt% MEA aqueous solution by conventional heating, which is around 120 °C.

3.3.2. Comparison of the desorption performance of AMP-based absorbents and MEA

As discussed above, AMP-based absorbents have demonstrated the excellent desorption performance. To further confirm their desorption capabilities and potential industrial application, the AMP-EG-DMF (4–3) is compared with 30 wt% aqueous amine solutions, specifically 30 wt% AMP-H₂O and 30 wt% MEA-H₂O. As illustrated in Fig. 7(a), at 90 °C, AMP-EG-DMF exhibited a remarkable desorption rate, which was approximately twice that of 30 wt% MEA-H₂O. This suggests that in anhydrous condition, the product of AMP-EG-DMF and CO_2 is much easier to decompose than CO_2 -AMP and CO_2 -MEA in aqueous condition.

The Fig. 7(b) summarizes the absorption capacity, desorption capacity, and regeneration efficiency of AMP-H₂O, MEA-H₂O, AMP-EG and AMP-EG-DMF (4–3), where the concentration of amines were kept at 30 wt%. These results indicate that, at the same desorption temperature, the non-aqueous absorbents (AMP-EG and AMP-EG-DMF) always exhibit higher regeneration efficiency than aqueous absorbents (AMP-H₂O and MEA-H₂O). Moreover, the addition of polar solvent into AMP-EG system further improve both the absorption capacity and regeneration efficiency significantly. MEA-H₂O, as a commonly used industrial CO_2 absorbents, demonstrated a high absorption capacity of 123 g- CO_2 / (kg-soln.), but its regeneration efficiency was only 56% at 90 °C. In contrast, the CO_2 absorption capacity of AMP-EG-DMF (4–3) is 122 g- CO_2 / (kg-soln.), which is slightly lower than that of MEA-H₂O, but its regeneration efficiency reaches to 98% at 90 °C. This means that the cyclic adsorption capacity of AMP-EG-DMF (4–3) is much higher than the benchmark absorbent MEA-H₂O, and has great potential to be applied in industry as energy-saving absorbent for CO_2 capture.

3.4. Volatilization and stability of absorbents

3.4.1. The cyclic experiments of AMP-based absorbents

Temperature is a critical factor affecting the CO_2 desorption. Obviously, higher temperature takes beneficial to desorption performance. Take AMP-DMF-EG as an example, from 50 to 90 °C, the desorption efficiency increased from 68.1% to 97.8% and the maximum desorption rate increased from 8.5 to 52.9 (g- CO_2 /kg-soln. ·min). Compared with 30 wt% MEA which usually requires about 120 °C to accomplish the desorption in the industry, AMP-based absorbents need lower temperature for regeneration. Thus, they greatly reduce energy consumption during the regeneration process.

To evaluate the stability of the AMP-EG-DMF system, cyclic absorption–desorption was conducted for seven times, and the results presented in Fig. 8. In each cycle, CO_2 absorption was at 25 °C for 50 min, CO_2 desorption or regeneration was at 90 °C for 30 min with N₂ gas purging. Notably, no solvent lost due to evaporation after the seven cycles. After 7 cycles of absorption–desorption, the cyclic CO_2 absorption capacity was 114.5 (g- CO_2 / kg-soln.), which is almost 94% of the maximum CO₂ adsorption capacity of AMP-DMF-EG. In contrast, for 30 wt% MEA, the CO₂ loading is about 123 (g- CO_2 / (kg-soln.)) for the first absorption, and then reduced to 75 (g- CO_2 / kg-soln.) at the 7th cycle which is only 61% of the initial absorption capacity. In addition, the AMP-DMSO-EG system has a cyclic performance similar to AMP-EG-DMF system as shown in Fig. S5. Therefore, the AMP-based absorbents exhibit much higher cyclic capacity and stability and higher CO₂ absorption/desorption efficiency than 30 wt% MEA aqueous solution.

3.4.2. The volatility of AMP-based absorbents

The Volatility is a critical criterion for amine selection for CO_2 capture from low pressure gas streams. The process of desorption occurs at approximately 90 °C, and the energy consumption is significantly impacted by the latent heat of evaporation. Fig. 9 shows the TG measurement of fresh and CO_2 -rich absorbents in a N₂ atmosphere at 90 °C for 40 min. The results indicate that the fresh AMP-DMF-EG absorbent experienced a weight loss of 8.3%, while the CO_2 -rich absorbent experienced a weight loss of 19.5%, attributed to partial CO_2 desorption. In contrast, the fresh and CO_2 -rich 30 wt% aqueous MEA absorbents showed significant weight loss of 61.2% and 74.2%, respectively. The low volatility of the AMP-DMF-EG absorbent can significantly reduce the absorbent's mass loss ratio and energy consumption due to the evaporation of solvent and water in a carbon capture process.

3.4.3. The thermal stability of AMP-based absorbents

The commercial application of absorbents requires good thermal stability. In general, the amine absorbents are exposed into heating for regeneration. Even though the desorption temperature of AMP-based absorbents (around 90 °C) is lower than MEA (120 – 140 °C), its thermal stability still needs to be assessed. The NMR and FT-IR are employed to characterize the fresh AMP-based absorbents, the AMP-based absorbents after one cycle, after three cycles, and after five cycles, respectively. The ¹³C NMR and ¹H NMR spectrum are shown in Fig. S6 and Fig. S7, and the FT-IR spectrum are shown in Fig. 10a. In each cycle, CO_2 absorption was at 25 °C for 50 min, CO_2 desorption or regeneration was

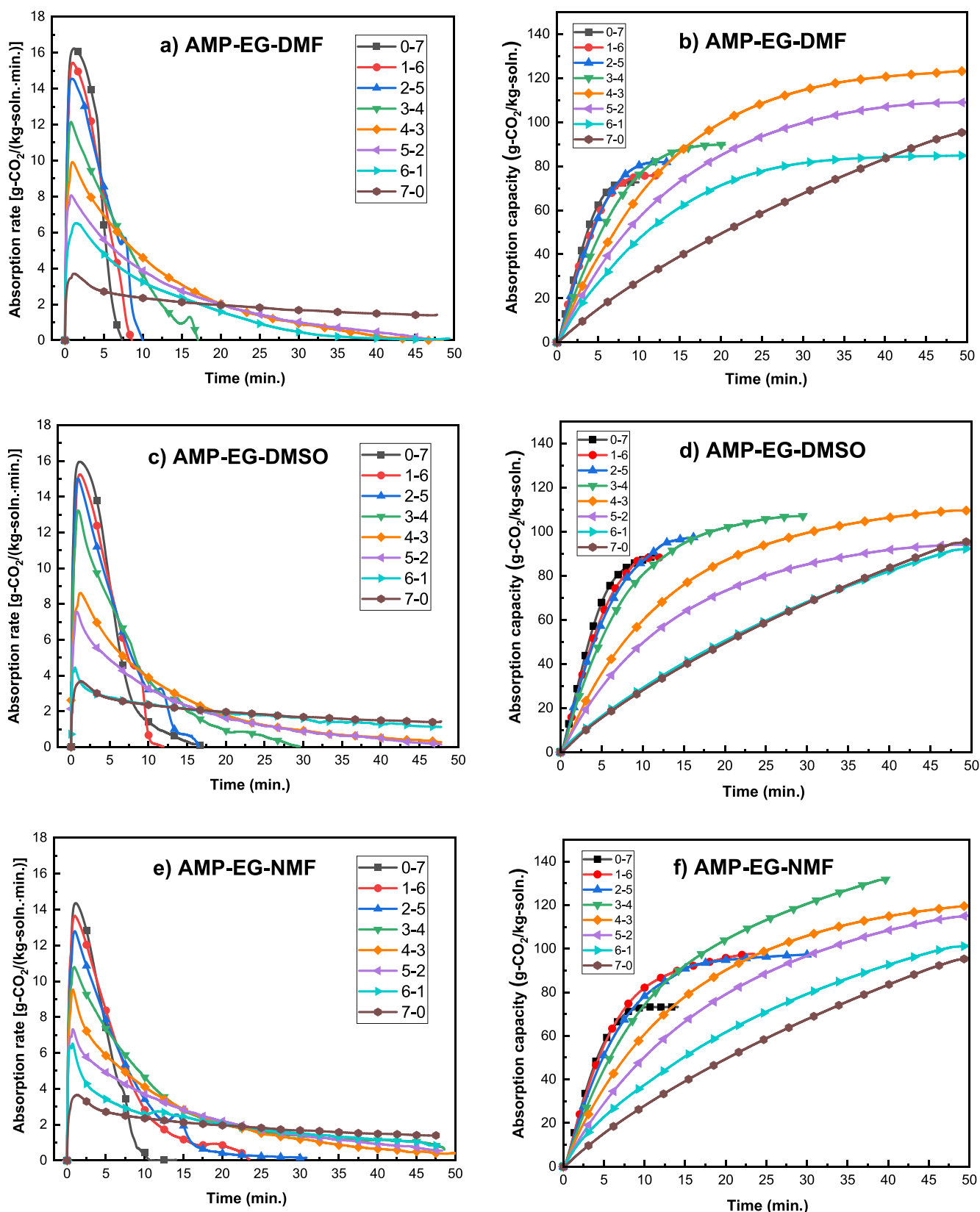


Fig. 3. CO_2 absorption profiles of bi-solvent AMP-based absorbents at 25°C. a-b) Absorption rate and CO_2 uptake of AMP-EG-DMF c-d) Absorption rate and CO_2 uptake of AMP-EG-NMF e-f) Absorption rate and CO_2 uptake of AMP-EG-DMSO.

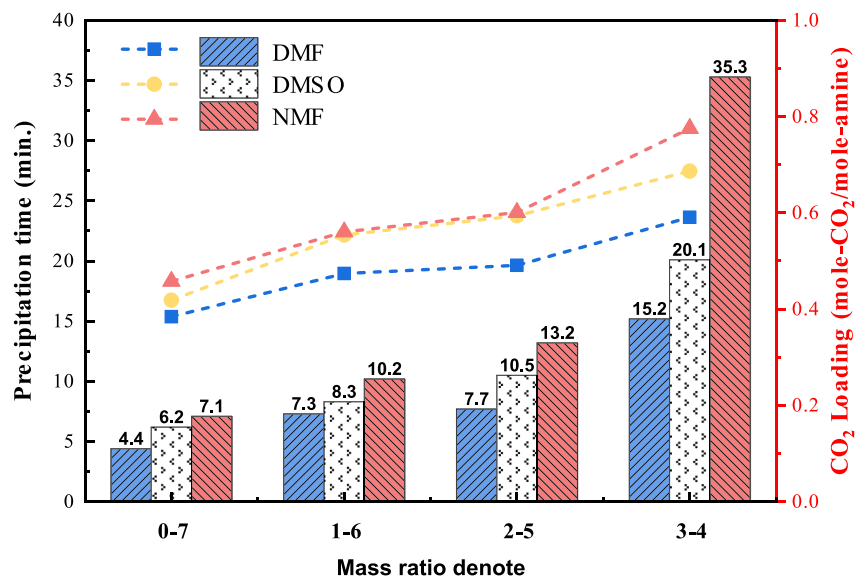


Fig. 4. Relationship between precipitation time of AMP-based absorbents and the EG mass ratio. The mass ratio denote is marked in Table 1.

Table 2

The summary of CO₂ absorption capacity, maximum CO₂ absorption rate and t₉₅ of AMP-based absorbents at 25°C.

Absorbents	Maximum CO ₂ absorption rate g-CO ₂ /kg-soln·min.	CO ₂ Capacity		t ₉₅ * min
		g-CO ₂ /kg-soln.	mole-CO ₂ /mole-amine	
AMP-EG-DMF (4-3)	9.91	122	0.82	32.0
AMP-EG-DMF (5-2)	7.96	110	0.74	34.5
AMP-EG-DMF (6-1)	7.49	101	0.68	39.0
AMP-EG-DMSO (4-3)	8.55	110	0.74	35.5
AMP-EG-DMSO (5-2)	8.77	104	0.70	36.5
AMP-EG-DMSO (6-1)	5.23	96	0.65	44.5
AMP-EG-NMF (4-3)	9.49	119	0.80	38.5
AMP-EG-NMF (5-2)	8.07	113	0.76	41.0
AMP-EG-NMF (6-1)	7.51	100	0.67	43.5
AMP-EG (7-0)	4.43	92	0.61	46.0
AMP-H ₂ O	6.04	95	0.63	34.2
MEA-H ₂ O	7.32	123	0.57	29.9

*:t₉₅ is the time spent on reaching 95% absorption capacity.

at 90 °C for 30 min with N₂ gas purging. The ¹³C NMR, ¹H NMR and ATR-FTIR spectrum showed that there are no new peaks or significant peak shift after multiple cycles, indicating that the AMP-based adsorbent not only has low evaporation but also good thermal stability. The chemical structures of AMP-based adsorbents are stable even when exposed to heat for regeneration.

3.5. The desorption energy consumption of AMP-based adsorbents

The high energy penalty is the major barrier for the implementation of CO₂ capture processes. AMP-based adsorbents developed in this study offer the potential for complete regeneration under mild conditions. To evaluate their specific energy consumption, both direct measurement and theoretic calculation are used to verify each other. The direct measurement of energy consumption is conducted through a microwave

swing process as detailed in section 2.2. The theoretic calculation is based on thermodynamic functions, including reaction heat, sensible heat, and latent heat. The reaction heat is measured using differential scanning calorimetry (DSC) [33]. Finally, the energy consumption of AMP-based adsorbents is compared to that of 30 wt% aqueous MEA.

3.5.1. Energy consumption measured from a microwave swing process

In CO₂ capture process, the high energy cost is primarily due to the regeneration of adsorbents [28]. In this work, CO₂ capture was conducted in a microwave swing system. As the energy consumption during microwave regeneration of adsorbents can be calculated through measuring the difference between the microwave energy before passing through the solvents and after passing the solvents. The detailed description of the principle can be seen in the Supporting Information Part 2. An ideal adsorbent for CO₂ treatment should exhibit a low energy/released CO₂ ratio, referred to as EC_t (Energy per CO₂ in kJ/mole), as defined by Eq. (8). A lower value of EC_t indicates the lower amount of energy consumed for the regeneration. As shown in Table 4, the EC_t value for MEA aqueous solution is the largest. The EC_t values decrease significantly after the addition of DMF, DMSO or NMF into AMP-EG to form bi-solvent adsorbents. Among the three AMP-based bi-solvent adsorbents, AMP-EG-DMF has the lowest EC_t, which is 67.5% lower than that of MEA-H₂O. This means that the energy consumption will reduce 67.5% if AMP-EG-DMF is used to replace the bench-mark solvent 30% MEA aqueous solution for CO₂ capture.

$$EC_t = \frac{Energy_t(kJ)}{CO_2\text{stripped}_t(mol)} \quad (8)$$

However, it should be noted that the microwave energies measured in this non-ideal microwave swing process are specific to the experimental setup used and cannot be directly compared to values from other literature. The microwave desorption energy measured for small samples, such as 5 g in this work, is known to overestimate the actual energy consumption required to strip CO₂. The data can only be used for the comparison of the energy consumption of different adsorbents. Additionally, the reactor was only partially heated by a microwave heater [15]; this leads to a high surface-to-volume ratio of the adsorbent, resulting in relatively high heat losses or evaporation rates. The heat extracted by the N₂ purging gas and the heat required to heat the quartz reactor also contribute to these energy losses. It is important to note that these energy losses are not exclusively utilized for CO₂ desorption but are accounted for in the reported data. Therefore, an energy

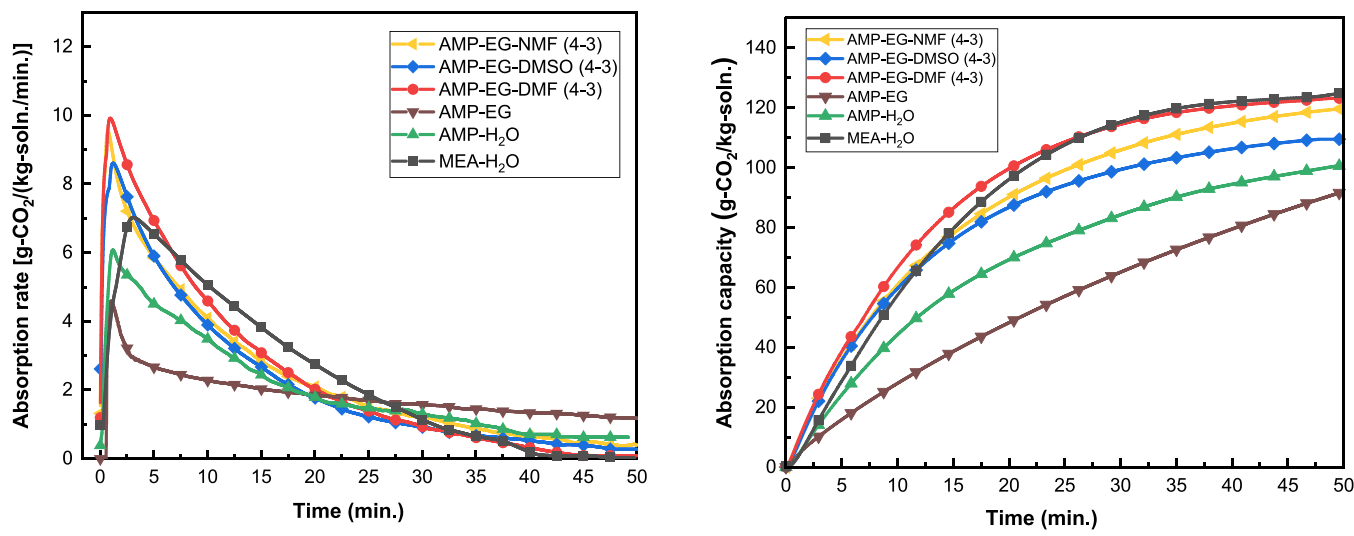


Fig. 5. Absorption performance of MEA-H₂O and AMP-based binary absorbents at 25°C. Left: Absorption kinetics. Right: Absorption capacity.

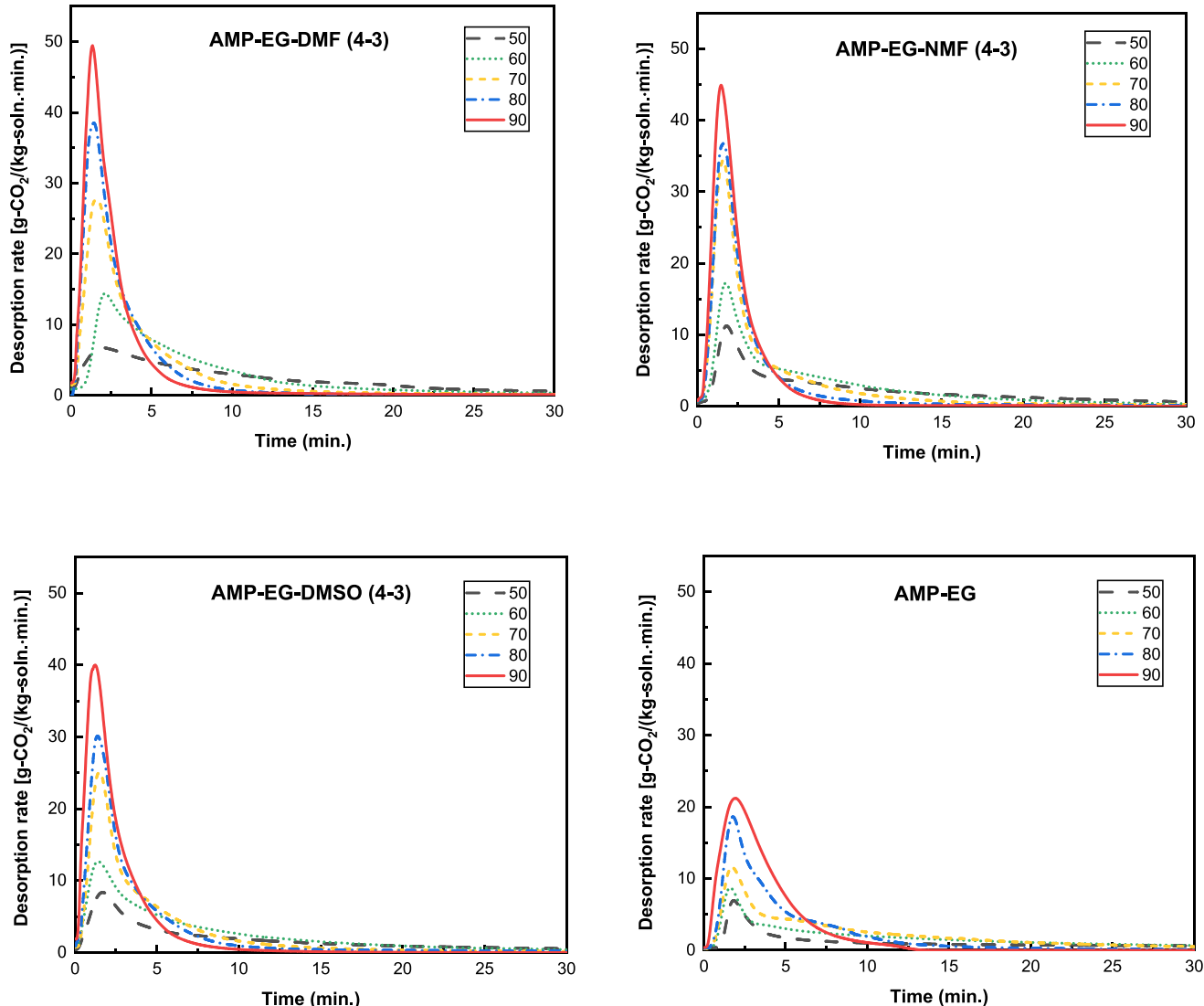


Fig. 6. CO₂ desorption profile of bi-solvent AMP-based absorbents. a) Desorption rate of AMP-EG-DMF b) Desorption rate of AMP-EG-NMF c) Desorption rate of AMP-EG-DMSO (4-3) d) Desorption rate of AMP-EG at 50-90°C.

Table 3

Desorption performance of AMP-EG-DMF/DMSO absorbents with various AMP to EG ratios.

Absorbent	Temp. °C	Maximum desorption rate g-CO ₂ / (kg-soln. min.)	CO ₂ desorbed g-CO ₂ /kg- soln.	Regeneration efficiency (η) %
AMP-EG-DMF (4-3)	50	8.5	84	68
	60	20.5	95	77
	70	34.1	105	86
	80	42.5	110	89
	90	52.9	119	98
AMP-EG- DMSO (4-3)	50	8.6	64	58
	60	13.2	84	76
	70	27.6	89	81
	80	31.2	94	86
	90	43.2	102	92
AMP-EG-NMF (4-3)	50	12.4	75	62
	60	19.2	88	73
	70	39.5	101	76
	80	41.3	91	82
	90	49.8	99	84
AMP-EG	50	7.2	51	53
	60	9.6	66	70
	70	11.4	74	80
	80	21.6	77	81
	90	22.8	82	89

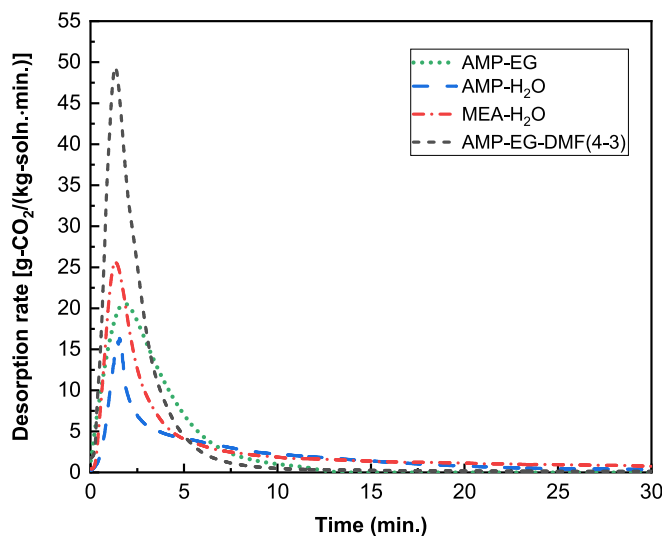


Fig. 7a. The comparison of CO₂ desorption kinetics of AMP-water, MEA-water, AMP-EG and AMP-EG-DMF absorbents at 90 °C.

consumption calculation approach based on the thermodynamics functions is proposed, following the ideal regeneration process.

3.5.2. Energy consumption calculated by thermodynamics functions

The energy (Q) during desorption process consists of three parts: the reaction heat of desorption (Q_r), the latent heat of vaporization (Q_v), and the sensible heat (Q_s). The calculation equations are shown below:

$$Q = Q_s + Q_r + Q_v \quad (9)$$

$$Q_s = \frac{C_p m_L \Delta T}{m_{CO_2}} = \frac{C_p \Delta T}{c_{ab} x M_{CO_2}} \quad (10)$$

$$Q_r = \frac{n_{CO_2} \Delta H}{m_{CO_2}} = \frac{\Delta H}{M_{CO_2}} \quad (11)$$

$$Q_v = \frac{n_w \Delta H_{H_2O}}{m_{CO_2}} = \frac{n_w \Delta H_{H_2O}}{n_{CO_2} M_{CO_2}} \quad (12)$$

Specific heat capacity (C_p) is needed for the calculation of the sensible heat (Q_s). In this study, the average heat capacities of AMP-EG, AMP-EG-DMF, AMP-EG-DMSO and AMP-EG-NMF systems are 170.53, 170.61, 173.10 and 161.89 (J/(mole*K)), respectively, and results of sensible heat are presented at Table 4. The specific heat capacity of the mixture is calculated from the sum of the specific heat capacities of the molar ratios of each component. The reaction heat takes up the largest part of regeneration energy, and has been measured by TG/DSC analyser. To ensure that the measured reaction heat is accurate, the reaction heat of 30 wt% aqueous MEA is measured first and the value is 1.892 kJ/g CO₂, which is consistent with the previous research (1.818–2.5 kJ/g CO₂) [32]. As shown in Fig. S4, the reaction heat for AMP-EG, AMP-EG-DMF, AMP-EG-DMSO and AMP-EG-NMF are 1.081, 0.807, 0.786, and 0.8104 kJ/g CO₂, respectively. Comparing to the reaction heat of 30 wt % aqueous MEA (1.892 kJ/g CO₂), the novel AMP-based absorbents developed in this study offer a substantial reduction in energy consumption for CO₂ capture. During the regeneration process, the energy required for vaporization (latent heat, (Q_v)) of the absorbent is significantly reduced. This is because the desorption temperature (90 °C) is considerably lower than the vaporization temperature of each component in the AMP-based absorbents, rendering the latent heat contribution negligible.

As seen in Table 5, according to previous report [33], the regeneration energy consumption value of 30 wt% MEA aqueous absorbent is 3.84 kJ/g CO₂. The Q_{total} of AMP-EG-DMF was 2.062 kJ/g CO₂, which was about 46.30% lower than that of MEA-H₂O and 35.50% lower than that of AMP-EG. For AMP based absorbents, the values of $Q_{sensibleheat}$ are much lower than that of MEA-H₂O. This could be attributed to the low heat capacity of EG. Similarly, the value of $Q_{reactionheat}$ for AMP-EG-DMF (0.807 kJ/g CO₂) was also lower than that for MEA-H₂O (1.795 kJ/g CO₂). The reduced energy consumption in CO₂ capture can be attributed to the instability of alkyl carbonates and their easier desorption characteristics.

In conclusion, the regeneration energy estimation is aligned to the EC_t calculation, that is the regeneration energy of AMP bi-solvent absorbents are lower than that of AMP with EG single solvent, and lower than that of MEA-H₂O. In comparison to MEA-H₂O, AMP-based absorbents can save about 16.74% to 46.30% energy in the CO₂ capture process, this characteristic makes it a promising and energy-saving alternative for CO₂ capture.

3.6. Reaction mechanism in AMP-based absorbents

Based on the zwitterion mechanism. CO₂ reacts with primary amines, such as AMP, to form zwitterions. Under non-aqueous conditions, the zwitterion further reacts with AMP through H⁺ transfer forming RHNCOO⁻, as illustrated in Eqs. (13)–(15) (RNH₂ denotes AMP). The stoichiometric coefficient of amine and CO₂ in the reaction is 2: 1 when a non-aqueous solvent is used. This means that the maximum CO₂ loading through this reaction is 0.5 mol CO₂ per mole amine [33,42].



However, for AMP-based absorbents developed in our studies (AMP-EG and bi-solvent non-aqueous AMP absorbents), the CO₂ loading could reach to 0.82 mol CO₂ per mole amine, which is much higher than the theoretical value of 0.5. To understand this significant improvement, the reaction mechanism of the AMP-based absorbents was investigated through qualitative analysis, employing in-situ Fourier Transform-Infrared (FT-IR) and Nuclear Magnetic Resonance (NMR) techniques.

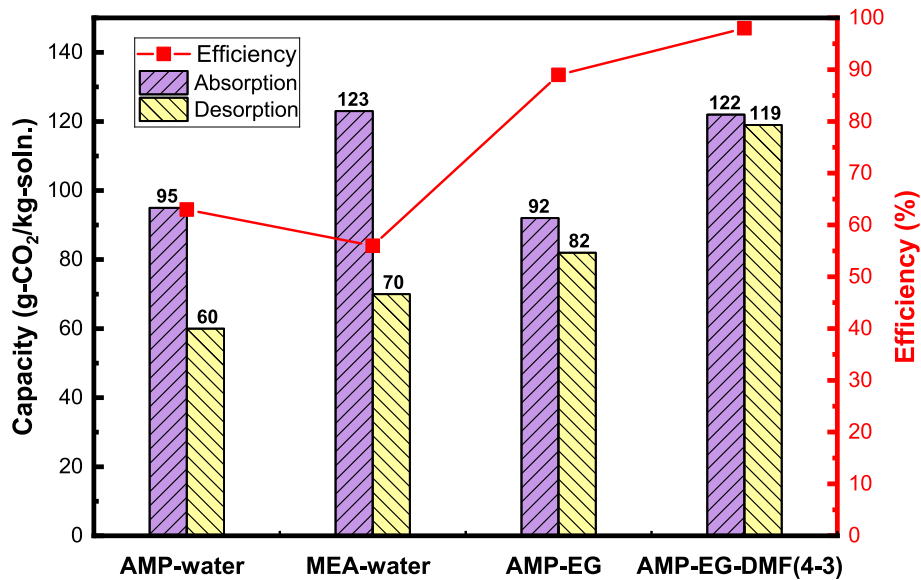


Fig. 7b. The comparison of CO₂ absorption/desorption capacity and regeneration efficiency of AMP-water, MEA-water, AMP-EG and AMP-EG-DMF absorbents at 90 °C.

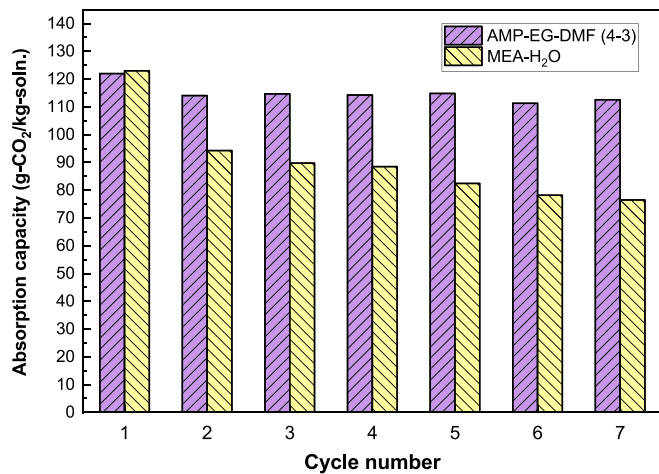


Fig. 8. Cyclic capacity of AMP-DMF-EG (4-3), compared with 30 wt% MEA-H₂O (Absorption: 25 °C, CO₂:20 ml/min N₂:80 ml/min; 50 min, desorption: 90 °C, N₂:100 ml/min; 30 min).

The NMR spectra are available in Fig. S9 and Fig. S10.

3.6.1. In-situ ATR FT-IR and NMR spectra

The ATR FT-IR were used to analyse the reaction products of the AMP based absorbents with CO₂ for a time interval of 0, 3, 5, 10, 20, 30 and 40 min to clarify the reaction mechanism. Additionally, the ¹³C NMR spectra of fresh and CO₂ saturated AMP-based absorbents are taken to verify AMP- CO₂ reaction products. The FT-IR spectra of the AMP-EG, AMP-EG-DMF, AMP-EG-DSMO and AMP-EG-NMF absorbents during CO₂ absorption are shown in Fig. 10b. The ¹³C and ¹H NMR spectra of AMP-based absorbents are shown in Fig. S9 and Fig. S10.

For AMP-EG binary absorbents as shown Fig. 10b, two additional peaks appeared in the region of 800–1700 cm⁻¹ in the FT-IR spectra of the reaction products. The 1520 cm⁻¹ peak is assigned to C = O asymmetric stretching in AMP-carbamate. The minor peak at 810 cm⁻¹ may be from C-N bending or torsions [43]. The ¹³C NMR results also confirmed the presence of AMP-carbamate at 162.89 ppm, which means that AMP-carbamate is the major product from CO₂ and AMP-EG binary absorbents. A small signal peak appeared at 159.37 ppm, indicating the

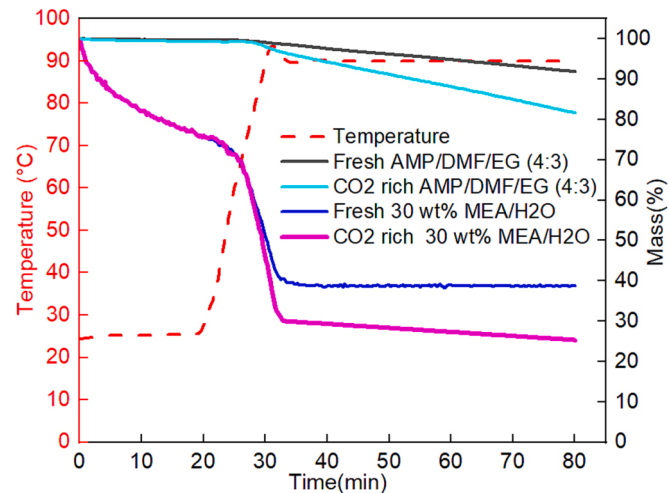


Fig. 9. TG results of the fresh and CO₂-rich (AMP-EG-DMF and 30 wt% aqueous MEA) absorbents.

presence of alkylcarbonate (R-O-COO⁻) [44]. However, the intensity of this peak was minimal, which demonstrated that only a small amount of EG reacted with CO₂. Therefore, for AMP-EG absorbents, CO₂ primarily reacts with AMP and forms AMP-carbamate, then some amount of CO₂ reacted with EG to form EG alkyl carbonate.

With the addition of the polar solvent (DMF, DMSO, or NMF), the reaction becomes much more complex, and the absorption capacity increased from 0.61 to 0.82 mol (CO₂)/mole (amine) due to the formation of new EG alkyl carbonate. Carbamate and bicarbonate formation, protonation of the amine group, and the dissolution of molecular CO₂ can be seen from the additional peaks, or the shift of existing peaks in their FT-IR spectra. In the case of AMP-EG-DMF, five new peaks appear at 759, 1178, 1290, 1460 and 1550 cm⁻¹ after CO₂ absorption. The 1550 and 1460 cm⁻¹ peaks were assigned to C = O asymmetric and symmetric stretching, which belongs to AMP-carbamate. The C-O and C-N stretching vibrations appeared at 1290 and 1178 cm⁻¹ peaks [43]. In ¹³C NMR spectrum, we observed that the carbamate and alkyl carbonate peaks appeared at 161.74 and 158.96 ppm. The ¹³C NMR peaks of AMP and EG shift, which can be attributed to the formation of AMP-

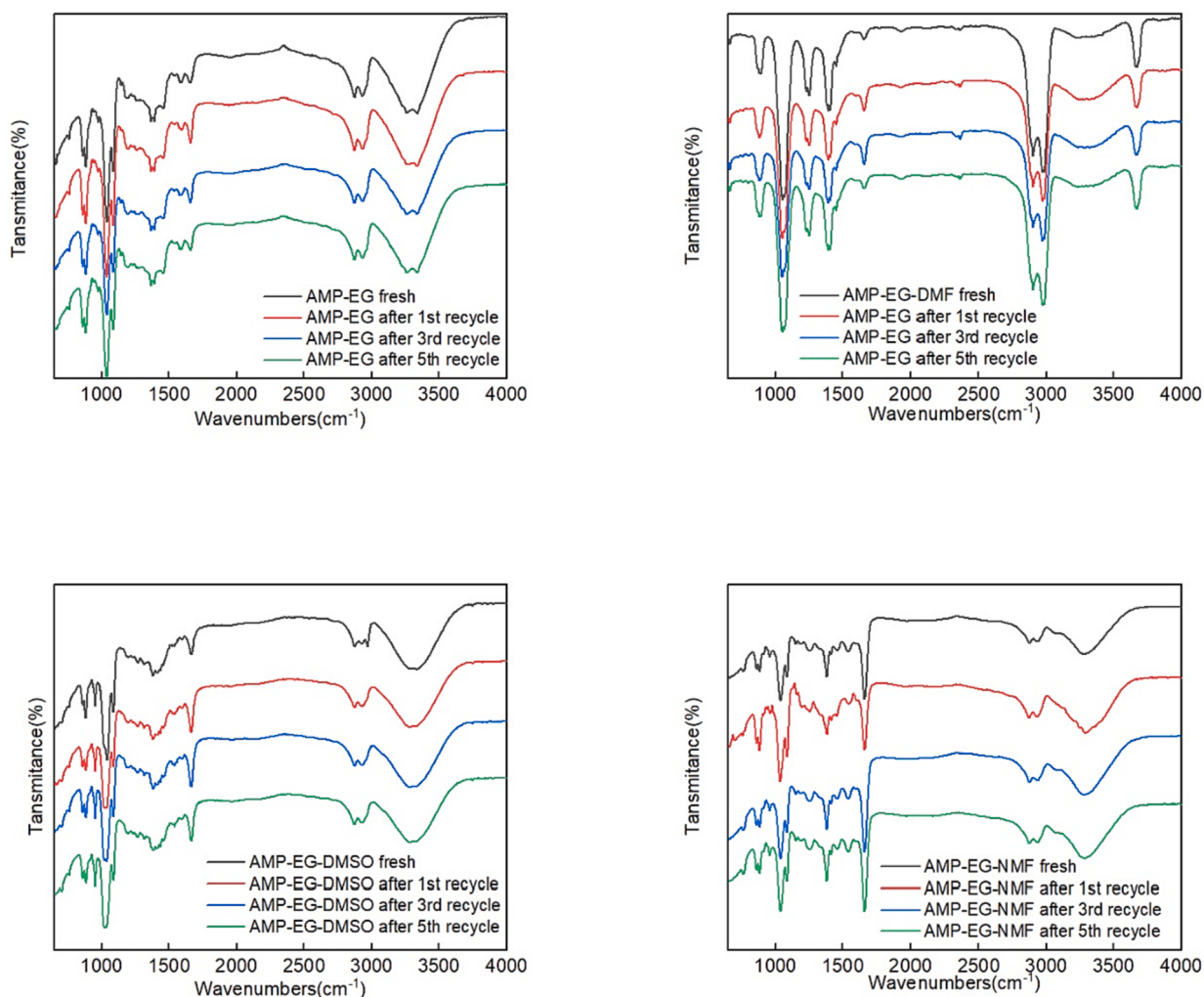


Fig. 10a. FT-IR spectrum of recycled AMP-based absorbents. From top left to right: AMP-EG and AMP-DMF-EG. From bottom left to right: AMP-DMF-EG and AMP-NMF-EG.

Table 4

The comparison of energy consumption of AMP-based absorbents and MEA absorbent at 90°C.

Absorbent with 30 wt% amine	AMP-EG	AMP-EG-DMF	AMP-EG-DMSO	AMP-EG-NMF	Aqueous 30 wt% MEA
Desorbed amount (mol)	0.00932	0.01351	0.01155	0.01127	0.00945
Energy (J)	3135.77	2698.82	3376.10	2653.27	5818.44
EC _i (kJ/mol)	319.4	199.7	292.3	235.2	615.3

Table 5

Regeneration energy of AMP-based absorbents and MEA estimated by thermodynamics equations.

Heat components	AMP-EG	AMP-EG-DMF	AMP-EG-DMSO	AMP-EG-NMF	Aqueous 30% MEA [33]
$C_p(\text{J}/(\text{mol}^{\circ}\text{K}))$	170.53	170.61	173.10	161.89	–
$Q_{\text{sensibleheat}}(\text{kJ/g CO}_2)$	2.116	1.255	1.397	1.305	1.961
$Q_{\text{reactionheat}}(\text{kJ/g CO}_2)$	1.081	0.807	0.786	0.810	1.795
$Q_{\text{vaporizationheat}}(\text{kJ/g CO}_2)$	0	0	0	0	0.068
$Q_{\text{total}}(\text{kJ/g CO}_2)$	3.197	2.062	2.183	2.115	3.84

carbamate and EG-alky carbonate, are shown in Fig. S9.

A similar IR and NMR spectrum could be observed during CO₂ absorption by AMP-EG-NMF solution, five similar peaks appear at 764, 1189, 1290, 1460 and 1543 cm⁻¹ after CO₂ absorption. The 1543 cm⁻¹ peaks were assigned to C = O asymmetric and symmetric stretching and it belongs to AMP-carbamate. The C-O and C-N stretching vibrations appeared at 1290 and 1189 cm⁻¹ peak. The ¹³C NMR spectroscopy of AMP-EG-NMF confirmed the presence of AMP-carbamate and alkyl carbonate of EG at 161.35 and 158.92 ppm. Additionally, the peak located at 164 ppm appeared in NMR spectrum of AMP-EG-DMF and AMP-EG-NMF belongs to the amide functional group of DMF/NMF [45].

As for AMP-EG-DMSO, the C-N stretching peak located at 1200 cm⁻¹ is disappeared in IR spectrum. It was because the C-N signal peak was shielded by sulfoxide group (1100–1200 cm⁻¹) [46] of DMSO, making it impossible to observe in the IR spectrum of the AMP-EG-DMSO solution. The ¹³C NMR spectrum of AMP-EG-DMSO also confirmed the presence of AMP-carbamate at 161.41 ppm and alkyl carbonate of EG at 159.32

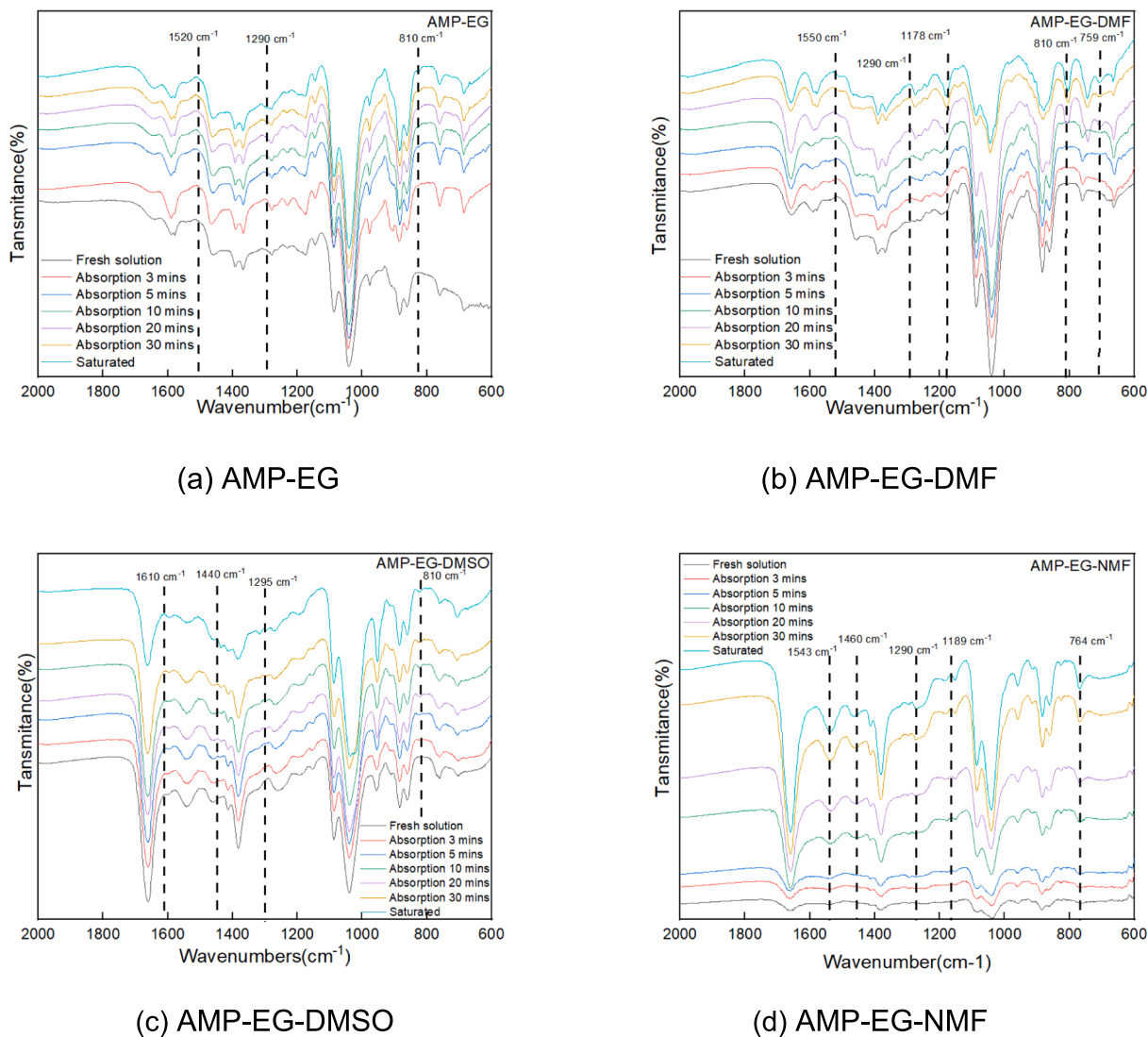


Fig. 10b. ATR-FTIR spectra of AMP based absorbents (0 min) and after bubbling CO_2 for 3, 5, 10, 20, 30 and 40 min.

ppm.

3.6.2. Density functional theory (DFT) calculations of AMP-based absorbents

Based on NMR and IR spectrum, it can be found that AMP-EG-DMF generates carbamate and alkyl carbonate after absorbing CO_2 . To further confirm the proposed absorption mechanism, DFT calculations were performed. For each set of calculations, the geometry and energy optimizations were performed at the B3LYP/6-311 + G (d, p) level [47]. The calculation results show that there is a possibility of AMPCOOH (AMP carbamic acid) in the reaction product. As shown in Fig. 11, in DMF-AMPCOOH mixture, the O—H—O hydrogen bond length between DMF and AMPCOOH is 1.761 Å, and the C—H—O hydrogen bond length is 2.243 Å. In DMSO-AMPCOOH mixture, the O—H—O hydrogen bond length between DMSO and AMPCOOH is 1.634 Å, and the two C—H—O hydrogen bond lengths are 2.311 and 2.315 Å, respectively. In NMF-AMPCOOH mixture, the O—H—O hydrogen bond length is 1.652 Å and the N—H—O hydrogen bond length is 1.809 Å. The hydrogen bond length in the three AMP-based solvents therefore take order: DMF-AMPCOOH > DMSO-AMPCOOH > NMF-AMPCOOH. The shorter the hydrogen bond, the greater the bond energy and the more stable the

structure. Hence, the results from DFT calculation are consistent with the experimental results, i.e., DMF- AMPCOOH is easier to regenerate than DMSO- AMPCOOH and NMF- AMPCOOH, therefore requires less energy consumption.

The NBO charge analysis is also used to calculate the free charge on the atom of the adsorbents. The results indicate that the negative charge of oxygen atom on DMSO is -0.950, which is the largest among the three solvents, therefore gives the shortest hydrogen bond. NMF has two negatively charged atoms, O and N. The charge of oxygen atom is -0.609 and the charge of nitrogen atom is -0.668. The combined effect of these two negatively charged atoms leads to a stable structure of AMPCOOH-NMF as well. However, DMF has only oxygen atom with a charge of -0.617, therefore leading to a relatively unstable structure and low regeneration energy required.

3.6.3. Summary of reaction mechanism

According to the theoretical analysis and experimental results, the possible CO_2 absorption mechanisms of AMP-EG and bi-solvent AMP based absorbents are proposed in Fig. 12. For AMP-EG absorbent, CO_2 absorption follows the zwitterion mechanism, in which CO_2 firstly reacts with AMP forming carbamate, then followed by the hydrolysis of

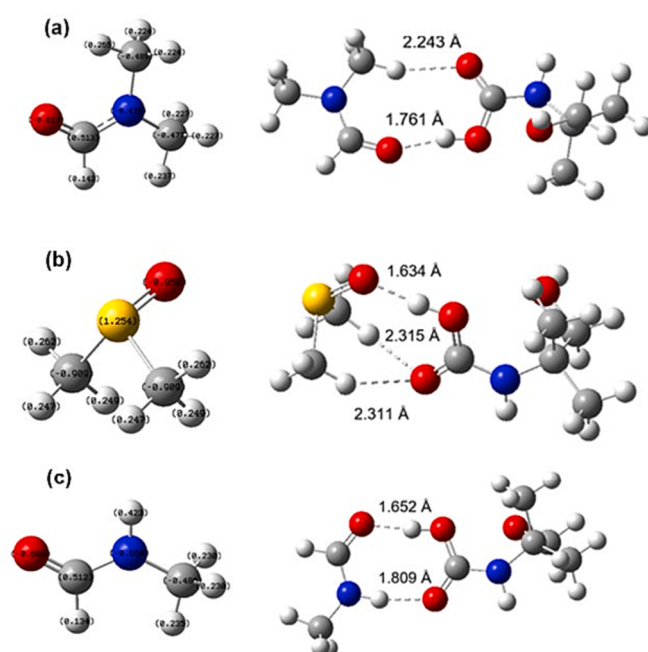


Fig. 11. NBO charge results and hydrogen-bonding interactions between AMP-carbamic acid and different polar solvents a) DMF b) DMSO c) NMF.

carbamate. The CO_2 uptake of AMP-EG is 0.61 (mole- CO_2 /mole-amine), which is slightly higher than the theoretical value of 0.5. This proves that part of CO_2 also reacted with EG. Due to the absence of H_2O in the

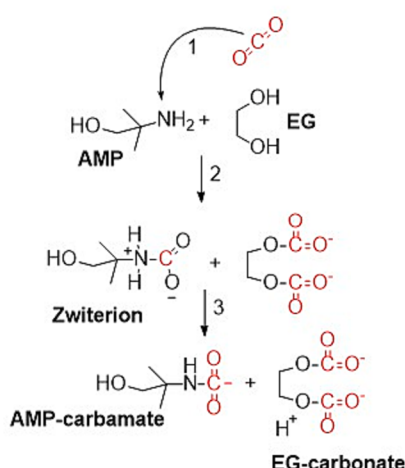
AMP-EG absorbent, CO_2 cannot be hydrated to form $\text{HCO}_3^-/\text{CO}_3^{2-}$.

With the addition of DMF, DMSO, or NMF to AMP-EG system, besides the formation of AMP-carbamate mentioned above, the hydroxyl group on EG is deprotonated and reacts with CO_2 forming alkyl carbonate due to the basic activation of AMP in the polar solvent. The addition of the polar solvents DMF, DMSO, or NMF to the AMP-EG system promotes the increase of 36.6% in the CO_2 absorption capacity from 92 (g- CO_2 /kg-soln.) to 122 (g- CO_2 /kg-soln.). DFT calculations also indicate that part of the carbamates could be converted into carbamic acid and stabilized by polar solvents (DMF/DMSO/NMF), therefore increase the absorption capacity. The synergistic effect of the bi-solvents enhances the absorption capacity and prevents precipitation. The reaction mechanism and routes are fully investigated and summarized in Fig. 12.

4. Conclusion and outlook

In this study, a novel strategy based on modifying electrostatic potential to prevent precipitation of CO_2 -adsorbent products is promoted to improve CO_2 absorption capacity and reduce the regeneration energy. We identified the cause of amine carbamate precipitation. Contrary to the commonly held belief that van der Waals forces play a dominant role in the reaction system, we found that electrostatic forces are the key factor in preventing the precipitation, and the addition of EG could effectively reduce electrostatic potential and prevent precipitation. Based on this strategy, AMP bi-solvent absorbents have been successfully developed for high efficiency of CO_2 capture with reduced regeneration energy consumption. The experimental results indicate that the bi-solvent strategy can compensate for each other's drawbacks in the developed AMP-based absorbents. The addition of polar solvents (DMF/DMSO/NMF) to AMP-EG enhances the CO_2 absorption rate and

The reaction route of AMP-EG with CO_2



The reaction route of AMP-DMF-EG with CO_2

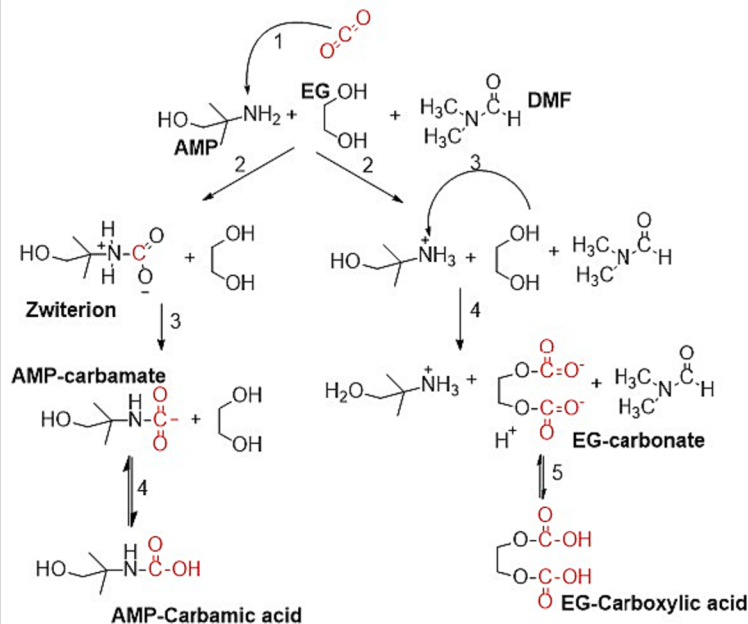


Fig. 12. The reaction mechanism between AMP-EG with CO_2 and AMP-EG-DMF with CO_2 .

capacity. Among these three solvents, the AMP-EG-DMF shows the best performance, including the highest absorption rate and capacity, the highest desorption rate, and the lowest regeneration efficiency. The optimal absorbent AMP-EG-DMF (4–3) exhibits 1.75 times higher regeneration efficiency than aqueous MEA with the same mass fraction (30 wt% AMP or MEA). The regeneration energy consumption of AMP-EG-DMF (4–3) is only 2.062 kJ/g CO₂, which is approximately 46.30% lower than the 3.84 kJ/g CO₂ of 30 wt% aqueous MEA. Moreover, this novel AMP-based bi-solvent absorbent also demonstrates excellent recycle stability and thermal stability, which is verified by TGA analysis. Based on In-situ FT-IR, NMR spectra and DFT calculation, it indicates that in AMP-EG binary system, CO₂ absorption follows the zwitterion mechanism. The CO₂ mainly reacts with AMP to form carbamate, and partially react with EG, resulting a slightly higher CO₂ absorption capacity than theoretical 0.5 (mole-CO₂/mole-amine). After the addition of polar solvents (DMF/DMSO/NMF) to AMP-EG system, part of the AMP-carbamate could be converted into carbamic acid and stabilized, which is verified by DFT calculation. The presence of EG also prevents precipitation of reaction products. The utilization of bi solvents to modify solvation free energy solubility provides new insights and strategy for developing next-generation amine absorbents for commercial applications in CO₂ capture with a low energy consumption.

Declaration of Competing Interest

The authors declare that they have no known competing financial interests or personal relationships that could have appeared to influence the work reported in this paper.

Data availability

Data will be made available on request.

Acknowledgement

This work was supported by Engineering and Physical Sciences Research Council (EP/V041665/1, EP/W027593/1).

Appendix A. Supplementary data

Supplementary data to this article can be found online at <https://doi.org/10.1016/j.cej.2023.145929>.

References

- [1] J.F.D. Tapia, J.Y. Lee, R.E.H. Ooi, D.C.Y. Foo, R.R. Tan, A review of optimization and decision-making models for the planning of CO₂ capture, utilization and storage (CCUS) systems, *Sustain. Prod. Consum.* 13 (Jan. 2018) 1–15, <https://doi.org/10.1016/J.SPC.2017.10.001>.
- [2] G.T. Rochelle, Amine scrubbing for CO₂ CAPTURE, *Science* 325 (5948) (2009) 1652–1654, <https://doi.org/10.1126/science.1176731>.
- [3] P.H.M. Feron, C.A. Hendriks, CO₂ capture process principles and costs, *Oil Gas Sci. Technol.* 60 (3) (2005) 451–459, <https://doi.org/10.2516/ogst:2005027>.
- [4] R.R. Bottoms, "Separating acid gases," *Girdler Corp.*, 1783901, 1930.
- [5] S.Y. Oh, M. Binns, H. Cho, J.K. Kim, Energy minimization of MEA-based CO₂ capture process, *Appl. Energy* 169 (2016) 353–362, <https://doi.org/10.1016/J.APENERGY.2016.02.046>.
- [6] K. Fu, W. Rongwong, Z. Liang, Y. Na, R. Idem, P. Tontiwachwuthikul, Experimental analyses of mass transfer and heat transfer of post-combustion CO₂ absorption using hybrid solvent MEA-MeOH in an absorber, *Chem. Eng. J.* 260 (Jan. 2015) 11–19, <https://doi.org/10.1016/J.CEJ.2014.08.064>.
- [7] S. Chen, S. Chen, Y. Zhang, L. Qin, C. Guo, J. Chen, Species distribution of CO₂ absorption/desorption in aqueous and non-aqueous N-ethylmonoethanolamine solutions, *Int. J. Greenh. Gas Control* 47 (Apr. 2016) 151–158, <https://doi.org/10.1016/J.IJGGC.2016.01.046>.
- [8] C. Guo, S. Chen, Y. Zhang, G. Wang, Solubility of CO₂ in nonaqueous absorption system of 2-(2-aminoethylamine)ethanol + benzyl alcohol, *J. Chem. Eng. Data* 59 (6) (Jun. 2014) 1796–1801, https://doi.org/10.1021/JE401028G/ASSET/IMAGES/MEDIUM/JE-2013-01028G_0010.GIF.
- [9] I.I.I. Alkhathib, L.M.C. Pereira, A. Alhajaj, L.F. Vega, Performance of non-aqueous amine hybrid solvents mixtures for CO₂ capture: a study using a molecular-based model, *J. CO₂ Util.* 35 (Jan. 2020) 126–144, <https://doi.org/10.1016/J.JCOU.2019.09.010>.
- [10] J. Tan, H. Shao, J. Xu, L. Du, G. Luo, Mixture absorption system of monoethanolamine–triethylene glycol for CO₂ capture, *Ind. Eng. Chem. Res.* 50 (7) (Apr. 2011) 3966–3976, <https://doi.org/10.1021/IE101810A>.
- [11] J. Li, C. You, L. Chen, Y. Ye, Z. Qi, K. Sundmacher, Dynamics of CO₂ absorption and desorption processes in alkanolamine with cosolvent polyethylene glycol, *Ind. Eng. Chem. Res.* 51 (37) (Sep. 2012) 12081–12088, <https://doi.org/10.1021/IE301164V>.
- [12] C.H. Yu, T.W. Wu, C.S. Tan, CO₂ capture by piperazine mixed with non-aqueous solvent diethylene glycol in a rotating packed bed, *Int. J. Greenh. Gas Control* 19 (Nov. 2013) 503–509, <https://doi.org/10.1016/J.IJGGC.2013.10.014>.
- [13] C. Zheng, J. Tan, Y.J. Wang, G.S. Luo, CO₂ Solubility in a Mixture Absorption System of 2-Amino-2-methyl-1-propanol with Glycol, *Ind. Eng. Chem. Res.* 51 (34) (Aug. 2012) 11236–11244, <https://doi.org/10.1021/IE3007165>.
- [14] T. Ping, Y. Dong, S. Shen, Energy-efficient CO₂capture using nonaqueous absorbents of secondary alkanolamines with a 2-butoxyethanol cosolvent, *ACS Sustain. Chem. Eng.* 8 (49) (Dec. 2020) 18071–18082, https://doi.org/10.1021/ACSSUSCHEMENG.0C06345/SUPPLFILE/SCOC06345_SI_001.PDF.
- [15] F. Bougie, D. Pokras, X. Fan, Novel non-aqueous MEA solutions for CO₂ capture, *Int. J. Greenh. Gas Control* 86 (Jul. 2019) 34–42, <https://doi.org/10.1016/j.ijggc.2019.04.013>.
- [16] F. Barzagli, C. Giorgi, F. Mani, M. Peruzzini, Reversible carbon dioxide capture by aqueous and non-aqueous amine-based absorbents: a comparative analysis carried out by 13C NMR spectroscopy, *Appl. Energy* 220 (March) (2018) 208–219, <https://doi.org/10.1016/j.apenergy.2018.03.076>.
- [17] H. Guo, C. Li, X. Shi, H. Li, S. Shen, Nonaqueous amine-based absorbents for energy efficient CO₂ capture, *Appl. Energy* 239 (Apr. 2019) 725–734, <https://doi.org/10.1016/j.apenergy.2019.02.019>.
- [18] K. Fu, C. Liu, L. Wang, X. Huang, D. Fu, Performance and mechanism of CO₂ absorption in 2-ethylhexan-1-amine + glyme non-aqueous solutions, *Energy* 220 (Apr. 2021), 119735, <https://doi.org/10.1016/J.ENERGY.2020.119735>.
- [19] L.v. Bihong, Y. Kexuan, Z. Xiaobin, Z. Zuoming, J. Guohua, 2-Amino-2-methyl-1-propanol based non-aqueous absorbent for energy-efficient and non-corrosive carbon dioxide capture, *Appl. Energy* 264 (2020) 114703.
- [20] H. Svensson, J. Edfeldt, V. Zejnullahu Velasco, C. Hultberg, H.T. Karlsson, Solubility of carbon dioxide in mixtures of 2-amino-2-methyl-1-propanol and organic solvents, *Int. J. Greenh. Gas Control* 27 (Aug. 2014) 247–254, <https://doi.org/10.1016/J.IJGGC.2014.06.004>.
- [21] Y. Li, J. Cheng, L. Hu, J. Liu, J. Zhou, K. Cen, Phase-changing solution PZ/DMF for efficient CO₂ capture and low corrosiveness to carbon steel, *Fuel* 216 (2018) 418–426.
- [22] X. Gao, X. Li, S. Cheng, B. Lv, G. Jing, Z. Zhou, A novel solid-liquid 'phase controllable' biphasic amine absorbent for CO₂ capture, *Chem. Eng. J.* 430 (Feb. 2022), 132932, <https://doi.org/10.1016/J.CEJ.2021.132932>.
- [23] X. Zhou, X. Li, J. Wei, Y. Fan, L. Liao, H. Wang, Novel nonaqueous liquid-liquid biphasic solvent for energy-efficient carbon dioxide capture with low corrosivity, *Environ. Sci. Tech.* 54 (24) (2020) 16138–16146, <https://doi.org/10.1021/acs.est.0c05774>.
- [24] X. Li, X. Zhou, J. Wei, Y. Fan, L. Liao, H. Wang, Reducing the energy penalty and corrosion of carbon dioxide capture using a novel nonaqueous monoethanolamine-based biphasic solvent, *Sep. Purif. Technol.* 265 (2021) 118481.
- [25] H.K. Karlsson, H. Makhool, M. Karlsson, H. Svensson, Chemical absorption of carbon dioxide in non-aqueous systems using the amine 2-amino-2-methyl-1-propanol in dimethyl sulfoxide and N-methyl-2-pyrrolidone, *Sep. Purif. Technol.* 256 (Feb. 2021), 117789, <https://doi.org/10.1016/J.SEPPUR.2020.117789>.
- [26] F.A. Chowdhury, K. Goto, H. Yamada, Y. Matsuzaki, A screening study of alcohol solvents for alkanolamine-based CO₂ capture, *Int. J. Greenh. Gas Control* 99 (2020) 103081.
- [27] V. Barbarossa, F. Barzagli, F. Mani, S. Lai, P. Stoppioni, G. Vanga, Efficient CO₂ capture by non-aqueous 2-amino-2-methyl-1-propanol (AMP) and low temperature solvent regeneration, *RSC Adv.* 3 (30) (Jul. 2013) 12349–12355, <https://doi.org/10.1039/C3RA40933C>.
- [28] J.D. Wagaarachige, Z. Idris, B. Arstad, N.B. Kummamuru, K.A.S. Sætre, M. Halstensen, K.-J. Jens, Low-viscosity nonaqueous sulfolane–amine–methanol solvent blend for reversible CO₂ capture, *Ind. Eng. Chem. Res.* 61 (17) (2022) 5942–5951.
- [29] S. Shen, X. Shi, C. Li, H. Guo, Q. Long, S. Wang, X. Yin, Nonaqueous (amine + glycol ether) solvents for energy-efficient CO₂ capture: New insights into phase change behaviors and assessment of capture performance, *Sep. Purif. Technol.* 300 (2022), 121908, <https://doi.org/10.1016/j.seppur.2022.121908>.
- [30] F. Bougie, X. Fan, Microwave regeneration of monoethanolamine aqueous solutions used for CO₂ capture, *Int. J. Greenh. Gas Control* 79 (July) (2018) 165–172, <https://doi.org/10.1016/j.ijggc.2018.10.008>.
- [31] S.J. McGurk, C.F. Martín, S. Brandani, M.B. Sweatman, X. Fan, Microwave swing regeneration of aqueous monoethanolamine for post-combustion CO₂ capture, *Appl. Energy* 192 (2017) 126–133, <https://doi.org/10.1016/j.apenergy.2017.02.012>.
- [32] X. Zhu, H. Lu, K. Wu, Y. Zhu, Y. Liu, C. Liu, B. Liang, DBU-Glycerol solution: A CO₂absorbent with high desorption ratio and low regeneration energy, *Environ. Sci. Tech.* 54 (12) (2020) 7570–7578.
- [33] W. Tian, K. Ma, J. Ji, S. Tang, S. Zhong, C. Liu, H. Yue, B. Liang, Nonaqueous MEA/PEG200 absorbent with high efficiency and low energy consumption for CO₂ capture, *Ind. Eng. Chem. Res.* 60 (10) (2021) 3871–3880.
- [34] M. J. Frisch et al., "G16_C01." p. Gaussian 16, Revision C.01, Gaussian, Inc., Wallin, 2016.

- [35] M.J. Al-Marri, M.M. Khader, E.P. Giannelis, M.F. Shibli, Optimization of selection of chain amine scrubbers for CO₂ capture, *J. Mol. Model.* 20 (12) (2014) 2518, <https://doi.org/10.1007/s00894-014-2518-8>.
- [36] P. Taylor, B. E. Roberts, A. E. Mather, and B. E. Roberts, "SOLUBILITY OF CO₂ AND H₂S IN A HINDERED AMINE SOLUTION," no. May 2013, pp. 37–41, 2007.
- [37] T. T. Tengf and A. E. Mather, "Solubility of CO₂ in an AMP Solution Excess Molar Volumes , Excess Logarithmic Viscosities , and Excess Activation Energies of Viscous Flow for 2-Ethoxyethanol + -Butyrolactone and + Sulfolane at 303 . 15 K," pp. 410–411, 1990.
- [38] E. Jo, Y.H. Jhon, S.B. Choi, J.-G. Shim, J.-H. Kim, J.H. Lee, I.-Y. Lee, K.-R. Jang, J. Kim, Crystal structure and electronic properties of 2-amino-2-methyl-1-propanol (AMP) carbamate, *Chem. Commun.* 46 (48) (2010) 9158.
- [39] I.O. Furtado, T.C. dos Santos, L.F. Vasconcelos, L.T. Costa, R.G. Fiorot, C. M. Ronconi, J.W.d.M. Carneiro, Combined theoretical and experimental studies on CO₂ capture by amine-activated glycerol, *Chem. Eng. J.* 408 (2021), 128002, <https://doi.org/10.1016/j.cej.2020.128002>.
- [40] F. Barzaghi, F. Mani, M. Peruzzini, Efficient CO₂ absorption and low temperature desorption with non-aqueous solvents based on 2-amino-2-methyl-1-propanol (AMP), *Int. J. Greenh. Gas Control* 16 (2013) 217–223, <https://doi.org/10.1016/j.ijggc.2013.03.026>.
- [41] T. Davran-Candan, DFT modeling of CO₂ Interaction with various aqueous amine structures, *Chem. A Eur. J.* 118 (25) (Jun. 2014) 4582–4590, <https://doi.org/10.1021/jp503929g>.
- [42] X.E. Hu, Q. Yu, F. Barzaghi, C. Li, M. Fan, K.A.M. Gasem, X. Zhang, E. Shiko, M. i. Tian, X. Luo, Z. Zeng, Y. Liu, R. Zhang, NMR techniques and prediction models for the analysis of species formed in CO₂ capture processes with amine-based sorbents: a critical review, *ACS Sustain. Chem. Eng.* 8 (16) (2020) 6173–6193.
- [43] M. Chen, M. Li, F. Zhang, X. Hu, Y. Wu, Fast and efficient CO₂ absorption in non-aqueous tertiary amines promoted by ethylene glycol, *Energy Fuel* 36 (9) (May 2022) 4830–4836, <https://doi.org/10.1021/acs.energyfuels.2c00215>.
- [44] D. Yang, M. Lv, J. Chen, Efficient non-aqueous solvent formed by 2-piperidinethanol and ethylene glycol for CO₂ absorption, *Chem. Commun.* 55 (83) (2019) 12483–12486, <https://doi.org/10.1039/c9cc06320j>.
- [45] M. Ando, A. Tashiro, M. Kawano, Y. Peng, T. Takamuku, H. Shirota, Exploring the microscopic aspects of 1-methyl-3-octylimidazolium tetrafluoroborate mixtures with formamide, N-methylformamide, and N, N-dimethylformamide by multiple spectroscopic techniques and computations, *J. Phys. Chem. B* 127 (17) (May 2023) 3870–3887, <https://doi.org/10.1021/acs.jpcb.2c09102>.
- [46] V.M. Wallace, N.R. Dhumal, F.M. Zehentbauer, H.J. Kim, J. Kiefer, Revisiting the Aqueous Solutions of Dimethyl Sulfoxide by Spectroscopy in the Mid- and Near-Infrared: Experiments and Car-Parrinello Simulations, *J. Phys. Chem. B* 119 (46) (Nov. 2015) 14780–14789, <https://doi.org/10.1021/acs.jpcb.5b09196>.
- [47] X. Gao, X. Li, S. Cheng, B. Lv, G. Jing, Z. Zhou, A novel solid–liquid ‘phase controllable’ biphasic amine absorbent for CO₂ capture, *Chem. Eng. J.* 430 (2022), 132932, <https://doi.org/10.1016/j.cej.2021.132932>.